Atmos. Chem. Phys. Discuss., 15, 27675–27748, 2015
www.atmos-chem-phys-discuss.net/15/27675/2015/
doi:10.5194/acpd-15-27675-2015

Atmospheric Chemistry and Physics Discussions
Open Access

Mediterranean desert dust outbreaks and their vertical structure based on remote sensing data

A. Gkikas[1], **S. Basart**[1], **N. Hatzianastassiou**[2], **E. Marinou**[3,9], **V. Amiridis**[3], **S. Kazadzis**[4,5], **J. Pey**[6], **X. Querol**[7], **O. Jorba**[1], **S. Gassó**[8], **and J. M. Baldasano**[1,8]

[1]Earth Sciences Department, Barcelona Supercomputing Center, Barcelona, Spain
[2]Laboratory of Meteorology, Department of Physics, University of Ioannina, Ioannina, Greece
[3]Institute for Astronomy, Astrophysics, Space Applications and Remote Sensing, National Observatory of Athens, Athens, 15236, Greece
[4]Physikalisch-Meteorologisches Observatorium Davos, World Radiation Center, Switzerland
[5]Institute of Environmental Research and Sustainable Development, National Observatory of Athens, Athens, Greece
[6]Spanish Geological Survey, Zaragoza IGME Unit, Zaragoza, Spain
[7]Institute of Environmental Assessment and Water Research, ID ÆA-CSIC C/Jordi Girona, 18–26, 08034 Barcelona, Spain
[8]Environmental Modelling Laboratory, Technical University of Catalonia, Barcelona, Spain
[9]Laboratory of Atmospheric Physics, Department of Physics, Aristotle University of Thessaloniki, Thessaloniki, Greece

Received: 20 July 2015 – Accepted: 8 September 2015 – Published: 14 October 2015

Correspondence to: A. Gkikas (antonis.gkikas@bsc.es)

Published by Copernicus Publications on behalf of the European Geosciences Union.

ACPD
15, 27675–27748, 2015

Abstract

The main aim of the present study is to describe the vertical structure of the intense Mediterranean dust outbreaks, based on the use of satellite and surface-based retrievals/measurements. Strong and extreme desert dust (DD) episodes are identified at $1^\circ \times 1^\circ$ spatial resolution, over the period March 2000–February 2013, through the implementation of an updated objective and dynamic algorithm. According to the algorithm, strong DD episodes occurring at a specific place correspond to cases in which the daily aerosol optical depth at 550 nm ($AOD_{550\,nm}$) exceeds or equals the long-term mean $AOD_{550\,nm}$ (Mean) plus two standard deviations (SD) value being smaller than Mean + 4 · SD. Extreme DD episodes correspond to cases in which the daily $AOD_{550\,nm}$ value equals or exceeds Mean + 4 · SD. For the identification of DD episodes additional optical properties (Ångström exponent, fine fraction, effective radius and Aerosol Index) derived by the MODIS-Terra & Aqua (also AOD retrievals), OMI-Aura and EP-TOMS databases are used as inputs. According to the algorithm using MODIS-Terra data, over the period March 2000–February 2013, strong DD episodes occur more frequently (up to 9.9 episodes yr^{-1}) over the western Mediterranean while the corresponding frequencies for the extreme ones are smaller (up to 3.3 episodes yr^{-1}, central Mediterranean Sea). In contrast to their frequency, dust episodes are more intense (AODs up to 4.1), over the central and eastern Mediterranean Sea, off the northern African coasts. Slightly lower frequencies and higher intensities are found when the satellite algorithm operates based on MODIS-Aqua retrievals, for the period 2003–2012. The performance of the satellite algorithm is assessed against surface-based daily data from 109 sun-photometric (AERONET) and 22 PM_{10} stations. The agreement between AERONET and MODIS AOD is satisfactory (R = 0.505–0.75) improving considerably when MODIS level 3 retrievals with higher sub-grid spatial representativeness and homogeneity are considered. Moreover, the evaluation analysis using other AERONET spectral optical and microphysical properties during the days of episodes as well as surface PM_{10} concentrations also provides strong support of the successful performance of the satellite algorithm. The CALIOP vertical profiles of pure and polluted dust observations and the associated total backscatter coefficient at 532 nm ($\beta_{532\,\mathrm{nm}}$), indicate that dust particles are mainly detected between 0.5 and 6 km, though they can reach 8 km between the parallels 32 and 38° N in warm seasons, while an increased number of CALIOP dust records at higher altitudes is observed with increased latitude, northwards to 40° N, revealing an ascending mode of the dust transport. However, the overall intensity of DD episodes is maximum (up to 0.006 $\mathrm{km}^{-1}\,\mathrm{sr}^{-1}$) below 2 km and at the southern parts of the study region (30–34° N). Additionally, the average thickness of dust layers gradually decreases from 4 to 2 km moving from south to north. In spring, dust layers of moderate-to-high $\beta_{532\,\mathrm{nm}}$ values ($\sim 0.004\,\mathrm{km}^{-1}\,\mathrm{sr}^{-1}$) are detected over the Mediterranean (35–42° N), extending from 2 to 4 km. Over the western Mediterranean, dust layers are observed between 2 and 6 km, while their base height is decreased down to 0.5 km for increasing longitudes underlying the role of topography and thermal convection. The vertical profiles of CALIOP $\beta_{532\,\mathrm{nm}}$ confirm the multilayered structure of the Mediterranean desert dust outbreaks on both annual and seasonal basis, with several dust layers of variable geometrical characteristics and intensities.

1 Introduction

The Mediterranean basin, due to its proximity to the major dust source arid areas of Northern Africa and Middle East (Middleton and Goudie, 2001; Prospero et al., 2002; Ginoux et al., 2012) is frequently affected by transported high dust loads referred to as episodes or events. The suspension and accumulation of mineral particles into the atmosphere over the Saharan and Arabian Peninsula's deserts are determined by various factors such as the enhanced turbulence, soil conditions (reduced vegetation cover and soil moisture), reduced precipitation amounts, latitudinal shift of the Intertropical Convergence Zone (ITCZ) as well as by small scale meteorological processes (e.g. haboobs). However, dust particles can be transported far away from their sources, mainly towards the Atlantic Ocean (e.g. Prospero and Lamb, 2003; Ben-Ami

ACPD
15, 27675–27748, 2015
3-D Mediterranean desert dust outbreaks
A. Gkikas et al.

et al., 2010; Huang et al., 2010) and Europe (e.g. Mona et al., 2006; Papayannis et al., 2008; Basart et al., 2012; Bègue et al., 2012; Pey et al., 2013), favored by the prevailing atmospheric circulation patterns, from planetary to synoptic scales. Due to their frequent transport in the Mediterranean, mineral dust particles, constitute the predominant aerosol type there (Barnaba and Gobbi, 2004; Basart et al., 2012), as shown by the good agreement, in spatial terms, between the geographical distributions of dust episodes' AOD (Gkikas et al., 2013) and average AOD conditions (Papadimas et al., 2008).

Dust particles play an important role for the shortwave (SW) and longwave (LW) radiation budget (e.g. Kaufman et al., 2002; Tegen et al., 2003; Heinold et al., 2008) and climate (IPCC, 2013). They affect atmospheric heating/cooling rates (e.g. Mallet et al., 2009) while they can also result in a modification of atmospheric dynamics and large atmospheric circulations like monsoons (e.g. Lau et al., 2006; Bollasina et al., 2011), cloud properties and precipitation (e.g. Huang et al., 2006; Solmon et al., 2008). Moreover, it has been shown that the consideration of their radiative impacts in numerical simulations can improve the forecasting accuracy of weather models (Pérez et al., 2006). Dust particles also affect air quality in urban areas (Basart et al., 2012) causing adverse health effects (Díaz et al., 2012; Karanasiou et al., 2012; Pérez García-Pando et al., 2014). All these consequences of dust aerosol are relevant and maximize under maximum dust loads, namely dust episodes, highlighting thus the significance of analyzing the spatial and temporal characteristics of such events. To this aim, many studies have been carried out using either surface (e.g. Cachorro et al., 2006) or satellite (e.g. Moulin et al., 1998) observations, as well as modelling techniques (e.g. Heinold et al., 2007) focusing on the broader Mediterranean area. These studies have been done either for specific cases (e.g. Kubilay et al., 2003; Balis et al., 2006) or for extended periods at specific locations (e.g. Meloni et al., 2007; Toledano et al., 2007a; Gobbi et al., 2013; Mona et al., 2014). Recently, Gkikas et al. (2013) developed an objective and dynamic algorithm relying on satellite retrievals, which enabled an overall view of dust episodes over the entire Mediterranean and the characterization of their regime.

ACPD
15, 27675–27748, 2015

Extensive research has been also carried out on the causes of Mediterranean dust outbreaks. Different mechanisms and processes of transport, apart from dust emissions in source areas, have been proposed as controlling factors. Moulin et al. (1997) showed that the exported dust loads from Northern Africa towards the Atlantic Ocean and the Mediterranean are controlled by the phase of the North Atlantic Oscillation (NAO). Other studies, focused on the description of atmospheric circulation characteristics favoring the occurrence of desert dust outbreaks over the central (Barkan et al., 2005; Meloni et al., 2008) or western (Querol et al., 1998; Rodriguez et al., 2001; Salvador et al., 2014) Mediterranean, but on a synoptic scale. An objective classification, based on multivariate statistical methods, of the atmospheric circulation patterns related to dust intrusions over the Mediterranean, has been presented by Gkikas et al. (2014) and Varga et al. (2014). The concentration of dust aerosols in the Mediterranean is characterized by strong spatial and temporal variability, associated with the seasonal variability of cyclones dominating or affecting the broader Mediterranean basin (Trigo et al., 2002). According to Moulin et al. (1998), dust AOD levels are higher in spring and summer compared to the wet seasons of the year. Moreover, dust intrusions are mainly recorded over the eastern Mediterranean in spring and winter, over the western parts in summer and over the central ones in autumn (Gkikas et al., 2013).

Dust transport over the Mediterranean is characterized by a multi-layered structure (Hamonou et al., 1999) in contrast to the Atlantic Ocean, which is well confined to the Saharan Air Layer (SAL, Karyampudi et al., 1999). The vertical distribution of dust particles into the troposphere and the profile of their physical and optical properties at different altitudes are controlling their impacts on atmospheric dynamics (Zhang et al., 2013). In order to describe the geometrical features of dust transport, many researchers have used ground lidar measurements, model simulations (Alpert et al., 2004; Kishcha et al., 2005) or they have relied on a synergistic use of satellite observations and ground lidar profiles (Berthier et al., 2006). The vertical extension of the Saharan dust intrusions over Europe, during the period 2000–2002, was the subject of a comprehensive study by Papayannis et al. (2008), who used lidar measurements from the EARLINET (European Aerosol Research Lidar Network, Bösenberg et al., 2003). Over the Mediterranean stations, the mean base, top and thickness of dust layers was found to vary from 1356 to 2980 m, 3600 to 5900 m and 726 to 3340 m, respectively. According to the obtained results, tracers of dust particles can be detected up to 10 km, as also reported by Gobbi et al. (2000), who studied a Saharan dust event in Crete (south Greece) during spring of 1999.

Several similar studies have been also performed for specific Mediterranean locations based on EARLINET lidar measurements. For example, Mona et al. (2006) analyzed the vertical structure of 112 Saharan intrusions that occurred over Potenza (Italy), from May 2000 to April 2003. The authors found that these outbreaks are confined between 1.8 and 9 km while their mass center is located at 3.5 km a.s.l. A similar analysis for Athens and Thessaloniki over the period 2000–2002, was conducted by Papayannis et al. (2005) who demonstrated that dust layers are recorded mainly between 2 and 5 km while their thicknesses vary from 200 to 3000 m. The geometrical characteristics of dust layers over Athens, during the period 2004–2006, have been also presented by Papayannis et al. (2009), who pointed out that the center of mass of dust layers is located at 2900 m being in a very good agreement with Kalivitis et al. (2007) findings (around 3 km) for the eastern Mediterranean. Additionally, the authors reported that the dust layers mainly extend from 1600 to 5800 m while mineral particles can be detected, at very low concentrations, up to 8 km a.s.l.. Gobbi et al. (2013) found that dust plumes, over Rome, mainly extend from 0 to 6 km while their center of mass is located at around 3 km. In the southern parts of Italy (Potenza), dust layers' base is found between 2 and 3 km, their geometrical height extends from 2.5 to 4 km while tracers of dust particles can be detected up to 10 km, based on a dataset of 310 dust events analyzed by Mona et al. (2014). Finally, Pisani et al. (2011) stated that the mean base and top of dust layers is found at 1500 and 4600 m a.s.l., respectively, while their mean thickness is equal to 3100 m, based on a statistical analysis of 45 desert dust episodes observed over Naples (Italy), from May 2000 to August 2003.

ACPD
15, 27675–27748, 2015

Surface-based lidar measurements like those used in the aforementioned studies provide useful information about the geometrical and optical properties of dust layers, but they are representative only for specific locations. Yet, a more complete knowledge about the vertical structure of dust outbreaks is necessary in order to adequately understand and determine their possible effects. The limitation imposed by the use of surface-based lidar observations can be overcome by utilizing accurate satellite retrievals, as a complementary tool, which provide extended spatial coverage. Since 2006, vertical resolved observations of aerosols and clouds from space were made possible thanks to the CALIOP (Cloud-Aerosol Lidar with Orthogonal Polarization) lidar flying onboard the CALIPSO (Cloud-Aerosol Lidar and Infrared Pathfinder Satellite Observations) satellite (Winker et al., 2009). Based on CALIOP observations, Liu et al. (2008) analyzed the global vertical distribution of aerosols for one year, while other studies focused on the vertical structure of dust outflows towards the Atlantic Ocean (e.g. Ben-Ami et al., 2009; Adams et al., 2012; Tsamalis et al., 2013) and the Pacific Ocean (e.g. Eguchi et al., 2009; Hara et al., 2009). On the contrary, over the broader Mediterranean area, only a small number of studies has been made aiming at describing the vertical distribution of dust aerosols (Amiridis et al., 2013) or specifying the vertical structure of dust events (Amiridis et al., 2009). Nevertheless, they only dealt with a single dust event (18–23 May 2008; Amiridis et al., 2009) and thus cannot satisfy the need to know the general vertical structure of Mediterranean dust episodes.

The main target of the present study is to describe the Mediterranean desert dust outbreaks' vertical structure over the period from March 2000 to February 2013. For this purpose, satellite retrievals derived by the MODIS-Terra/Aqua, Earth Probe-TOMS, OMI-Aura and CALIOP-CALIPSO databases (Sect. 2) are used in a synergistic way. The dust outbreaks are identified with an objective and dynamic algorithm, which uses appropriate aerosol optical properties representative of suspended particles' load, size and nature (Sect. 3). Based on its outputs, the primary characteristics of the intense Mediterranean desert dust (DD) episodes, namely their frequency and intensity, are described in Sect. 4.1. The performance of the satellite algorithm is evaluated in detail against surface measurements provided by AERONET or PM_{10} stations, located within the study region (Sect. 4.2). Additionally, useful information about various optical and physical properties under intense dust episodes conditions is also derived from the evaluation analysis. For the identified DD episodes, collocated CALIOP-CALIPSO vertical feature mask and total backscatter coefficient retrievals are used in order to describe the annual and seasonal variability of dust outbreaks' vertical extension over the Mediterranean (Sect. 4.3). Finally, the summary and conclusions are drawn in Sect. 5.

2 Satellite and surface-based data

The different types of satellite retrievals that have been used as inputs to the objective and dynamic satellite algorithm are described below, namely MODIS (Sect. 2.1.1), EP-TOMS and OMI-Aura (Sect. 2.1.2) databases. Also, CALIOP-CALIPSO vertically resolved satellite data, coincident with the identified desert dust outbreaks by the satellite algorithm, are described in Sect. 2.1.3. Finally, surface-based sun-photometric AERONET retrievals and PM_{10} concentrations, both used to assess the performance of the satellite algorithm, are described in Sect. 2.2.1 and 2.2.2, respectively.

2.1 Satellite data

2.1.1 MODIS

MODerate resolution Imaging Spectroradiometer (MODIS) onboard the Terra and Aqua satellites – with daytime local equator crossing time at 10:30 and 13:30, respectively, and 2330 km viewing swath – acquires measurements at 36 spectral bands between 0.415 and 14.235 µm with spatial resolution of 250, 500 and 1000 m. Observations from Terra and Aqua are made continuously since February 2000 and July 2002, respectively, and are available from the LAADS website (ftp://ladsweb.nascom.nasa.gov/). Aerosol optical properties are retrieved through the Dark Target (DT) algorithm (see e.g. Kaufman et al., 1997, 2001; Tanré et al., 1997; Levy et al., 2003; Remer et al.,

ACPD
15, 27675–27748, 2015

2005) where different assumptions are considered depending on the underlying surface type (land or ocean). Several evaluation studies (e.g. Remer et al., 2008; Papadimas et al., 2009; Levy et al., 2010; Nabat et al., 2013) have shown that aerosol optical depth (AOD) can be retrieved satisfactorily by MODIS, nevertheless its performance is better over sea (uncertainty equal to $\pm 0.03 \pm 0.05 \times$ AOD, Remer et al., 2002) than over land ($\pm 0.05 \pm 0.15 \times$ AOD, Levy et al., 2010).

The following daily MODIS-Terra and MODIS-Aqua Collection 051 (C051) level 3 satellite data (MOD08_D3 and MYD08_D3 files) provided at $1^{\circ} \times 1^{\circ}$ latitude–longitude spatial resolution are used: (i) $AOD_{550\,nm}$, (ii) Ångström exponent over land ($\alpha_{470-660\,nm}$), (iii) Ångström exponent over ocean ($\alpha_{550-865\,nm}$), (iv) fine-mode fraction (FF) of AOD over land and ocean and (v) Effective radius over ocean (r_{eff}). Similar data have been used by Gkikas et al. (2013), however, in the present study we have improved data quality by using the quality assurance-weighted (QA) data only (http://modis-atmos.gsfc.nasa.gov/_docs/QA_Plan_2007_04_12.pdf). Moreover, the day cloud fraction as well as the number of level 2 counts, which are both relevant to the performance of the satellite algorithm, are also used in this study. The time series of daily MODIS aerosol data cover the 13 yr period March 2000–February 2013 (Terra) and the 10 yr period January 2003–December 2012 (Aqua).

2.1.2 EP/TOMS and OMI-Aura

The selected retrievals from MODIS provide information about particles' load and size, which are both necessary to identify dust episodes. However, since dust is not the only coarse aerosol, for example sea-salt can be so as well, another optical property indicative of particle absorption efficiency is also required by the algorithm. To address this issue, the Absorption Aerosol Index (AI) daily data were also used, derived from measurements taken by the Total Ozone Mapping Spectrometer (TOMS) onboard the NASA's Earth-Probe satellite and the Ozone Monitoring Instrument (OMI) instrument onboard the NASA's Aura satellite. AI is the primary TOMS aerosol product (Herman et al., 1997) based on a spectral contrast method in a UV region (331–

ACPD
15, 27675–27748, 2015

360 nm) where ozone absorption is very small and can be used for the distinction between scattering (e.g. sea-salt) and absorbing (e.g. desert dust, smoke, volcanic ash) aerosols. The retrieval algorithm (fully described by Torres et al., 1998, 2002, 2005) takes advantage of the low surface albedo in the UV spectrum range, even in arid and semi-arid areas, making thus possible the estimation of the AOD over highly reflecting desert surfaces, where the major dust sources are located. Since the late 70's, the TOMS sensor onboard Nimbus-7 (1978–1993) and Earth Probe (1996–2005) has been providing global aerosol measurements. With the deployment of the EOS-Aura OMI (Ozone Monitoring Instrument) in mid-2004 (Torres et al., 2007) the near UV aerosol record continues to be extended into the foreseeable future. OMI is a hyperspectral sensor, covering the 270–500 nm range, launched onboard the EOS-Aura satellite on 15 July 2004 (13:38 equator crossing time, ascending mode) providing almost daily global coverage thanks to its wide viewing swath (2600 km with 13 km × 24 km nadir resolution). Apart from AI measurements, OMI aerosol products include also the total and absorption AOD and the single scattering albedo at 388 and 500 nm (Torres et al., 2007). Both EP-TOMS and OMI-Aura retrievals are available via the Mirador ftp server (http://mirador.gsfc.nasa.gov/) of the Goddard Earth Sciences Data and Information Services Center (GES DISC).

2.1.3 CALIOP-CALIPSO

The Cloud-Aerosol Lidar with Orthogonal Polarization (CALIOP) onboard the NASA's satellite CALIPSO (Cloud-Aerosol Lidar and Infrared Pathfinder Satellite Observations), launched in April 2006, provides vertical resolved aerosol and cloud observations (Winker et al., 2009) since June 2006. CALIPSO is flying in the A-Train constellation (Stephens et al., 2002; http://atrain.nasa.gov/) in a sun-synchronous polar orbit at 705 km over the surface, with a 16-day repeat cycle, crossing the equatorial plane at about 13:30 LST (Winker et al., 2009). CALIOP is an active sensor measuring the backscatter signal at 532 and 1064 nm as well as the polarization at 532 nm (Winker et al., 2009). These level 1 retrievals are further processed (calibra-

ACPD
15, 27675–27748, 2015

tion and range corrections) passing to Level 2 in order to retrieve the backscatter and extinction coefficients, at 532 and 1064 nm, for aerosol and cloud layers. The identification of cloud and aerosol layers within the atmosphere (Vaughan et al., 2009) is made through the cloud aerosol discrimination (CAD) algorithm (Liu et al., 2009), which is based on the probability distribution functions (PDFs) of altitude-and-latitude-dependent parameters (integrated color ratio, layer-integrated volume depolarization ratio, mean attenuated backscatter coefficient). CAD scores vary mainly from −100 to 100 indicating the presence of aerosols and clouds when are negative and positive, respectively, while bins of confidence levels, both for aerosols and clouds, are defined based on their absolute values (https://eosweb.larc.nasa.gov/sites/default/files/project/calipso/quality_summaries/CALIOP_L2VFMProducts_3.01.pdf). Aerosols are categorized in 6 primary types namely: (i) clean marine, (ii) dust, (iii) polluted continental, (iv) clean continental, (v) polluted dust and (vi) smoke (Omar et al., 2009).

In the present analysis, we use the Version 3 (3.01 and 3.02) of the Level 2 Vertical Feature Mask (VFM) and Aerosol Profile Products (APro) files, available from June 2006 to February 2013, both derived from the NASA's Earth Observing System Data and Information System (http://reverb.echo.nasa.gov/). The aerosol profile products are generated at a uniform horizontal resolution of 5 km (http://www-calipso.larc.nasa.gov/products/CALIPSO_DPC_Rev3x6.pdf), while the vertical resolution varies from 60 to 180 m depending on the altitude range and the parameter. The scientific data sets which have been analyzed are the following: (i) aerosol subtype, (ii) CAD score and (iii) total backscatter coefficient at 532 nm ($\beta_{532\,\mathrm{nm}}$), reported at several tropospheric and stratospheric levels above mean sea level (Hunt et al., 2009).

2.2 Surface-based data

2.2.1 AERONET

The AErosol RObotic NETwork (AERONET, Holben et al., 1998) is a worldwide network of installed CIMEL sun-sky radiometers obtaining sun-photometric observations

ACPD
15, 27675–27748, 2015

in more than 1000 locations of the planet (http://aeronet.gsfc.nasa.gov). The solar irradiances received by the photometer are inversed to columnar aerosol optical and microphysical properties through the implementation of retrieval algorithms (e.g. Dubovik and King, 2000; O'Neill et al., 2003). The followed standardized methods concerning instrument maintenance, calibration, cloud screening and data processing allow aerosol monitoring and comparison between different study periods and areas (Smirnov et al., 2000). From the global AERONET stations, 109 are located within the geographical limits of our study region. For each station, the daily averages of cloud-screened and quality assured data (Level 2.0) of direct sun and almucantar retrievals are used for: (i) AOD at 7 wavelengths from 340 to 1020 nm, (ii) size distribution retrieved for 22 logarithmically equidistant discrete points (r_i) in the range of sizes 0.05 µm ≤ r ≤ 15 µm, (iii) Ångström exponent between 440 and 870 nm ($\alpha_{440-870\,\mathrm{nm}}$), (iv) total effective radius (r_{eff}), and (v) single scattering albedo (SSA) and asymmetry parameter (g_{aer}) both retrieved at 440, 675, 870 and 1020 nm. The uncertainty in the estimation of AOD depends on technical (e.g. calibration method) factors and inversion assumptions, both described in detail in Holben et al. (1998). Moreover, the accuracy of the retrieved AOD by the CIMEL radiometer is spectrally dependent, being higher ($< \pm 0.01$) for wavelengths longer than 440 nm and lower ($< \pm 0.02$) for UV wavelengths (Eck et al., 1999). It should be also noted that the AERONET Level 2.0 inversion products (e.g. SSA) are provided when AOD at 440 nm is higher than 0.4 ensuring the minimization of the inversion uncertainties, which are also determined by other factors (e.g. scattering angle, particles' sphericity) as stated in detail by Dubovik et al. (2000).

2.2.2 PM_{10}

Daily total and dust surface PM_{10} concentrations, over the period 2001–2011 from 22 regional background and suburban background sites were used in this study. The monitoring sites are distributed as follow: 10 are located in Spain; 2 are in southern France; 5 are in Italy; 3 are in Greece; 1 is in southern Bulgaria and 1 is in Cyprus. PM_{10} concentrations were obtained in most cases from gravimetric determinations on

ACPD
15, 27675–27748, 2015

filters, whereas in few cases they were determined by real time instruments (Querol et al., 2009b; Pey et al., 2013) but corrected against gravimetric measurements carried out in annual field campaigns. The disaggregation of the dust component to the total amount is made based on a statistical approach which has been applied in several past studies (e.g. Rodríguez et al., 2001; Escudero et al., 2007; Querol et al., 2009b; Pey et al., 2013). A full description of the methodology which is followed for the calculation of dust particles' contribution to the total PM_{10} is presented in Escudero et al. (2007). Briefly, the net dust PM_{10} amount is calculated through the subtraction of the regional background PM_{10}, which is obtained by applying a monthly moving 30 percentile to the PM_{10} timeseries excluding days of dust transport, from the corresponding values of the total PM_{10} concentrations. The derived data were obtained from public European databases: AirBase (http://acm.eionet.europa.eu/databases/airbase/), EMEP (www.emep.int/) and EUSAAR (http://www.eusaar.net/).

3 Identification of desert dust episodes

Following the methodology proposed by Gkikas et al. (2013), desert dust (DD) episodes are identified based on an objective and dynamic algorithm, which is depicted in the flowchart of Fig. 1. The algorithm operates in three steps and is applied in each $1^\circ \times 1^\circ$ geographical cell. First (Fig. 1, yellow box), the mean (Mean) and the associated standard deviation (SD) of $AOD_{550\,nm}$ are calculated for the whole study period. These primary statistics are used for the definition of two threshold levels, which are equal to $Mean + 2 \cdot SD$ and $Mean + 4 \cdot SD$. At the next step, the algorithm analyzes the daily $AOD_{550\,nm}$ timeseries and classifies an episode as a strong one when AOD is between the two defined thresholds ($Mean + 2 \cdot SD \leq AOD_{550\,nm} < Mean + 4 \cdot SD$) and as an extreme one when AOD is higher/equal than $Mean + 4 \cdot SD$ (cyan boxes). The same approach was undertaken by Gkikas et al. (2009) who classified the Mediterranean aerosol episodes over the period 2000–2007 according to their strength and described their frequency and intensity. It must be clarified that according to our methodology in areas frequently affected by dust episodes, both mean and standard deviation values are expected to be high resulting to high thresholds which means that cases with relatively high AODs, relevant to radiative and health effects, are masked out from the dataset. Moreover, it must be mentioned that the satellite algorithm identifies only intense desert dust episodes since their AOD must be higher than Mean + 2 · SD which is considered as a high threshold level. In a further step of the methodology, the strong and extreme DD episodes are identified separately over land and sea surfaces of the study region. This is achieved through the usage of specific aerosol optical properties, namely the Ångström exponent, effective radius, fine fraction and aerosol index, which provide information about particles' size and nature (black box). For each optical property, appropriate upper or lower thresholds have been set up (green boxes) in order to certify the presence of dust particles in the atmosphere. These cut-off levels have been selected according to the literature findings, availability of raw data and several sensitivity tests (more details are provided in Gkikas et al., 2013). The validity of these thresholds is further evaluated against AERONET measurements and the corresponding results are discussed in Sect. "Intercomparison of surface-based and satellite algorithms used for the identification of the desert dust episodes".

As explained, a similar methodology and data were used in the study by Gkikas et al. (2013). Nevertheless, the present one is a significant extension mainly for three reasons: (i) DD episodes are identified here over an extended period of study and for both MODIS platforms, i.e. March 2000–February 2013 for MODIS-Terra and 2003–2012 for MODIS-Aqua, (ii) the quality of results is improved by using QA-weighted level-3 data produced by weighting level-2 data based on their confidence flag instead of regular ones (QA> 1) used in Gkikas et al. (2013) and (iii) emphasis is given to the vertical structure of the intense DD episodes. Moreover, in the present version of the algorithm are not implemented temporal filters, concerning the availability (masking out of AOD grid cells with less than 50 % available data of the timeseries) of raw AOD data, in contrast to Gkikas et al. (2009, 2013). Another improvement of the methodology consists in the application of our satellite algorithm also using only AODs associated with cloud fractions (CF) lower/equal than 0.8, in order to investigate possible modifications of our results due to the cloud contamination effects on MODIS AODs. The critical value of 0.8 for CF has been defined according to Zhang et al. (2005) and Remer et al. (2008), who stated that under extended cloud coverage conditions AOD levels can be increased substantially.

4 Results

Before dealing with the vertical structure of dust outbreaks (Sect. 4.3), it is very important to describe their horizontal patterns (Sect. 4.1) and also to assess the satisfactory algorithm's performance through a comparison against quality AERONET and PM_{10} observations (Sect. 4.2) in order to ensure an accurate three-dimensional view of the intense Mediterranean DD episodes. The present section has been organized accordingly and the results are given below.

4.1 2-D geographical distributions of desert dust episodes' frequency and intensity

The mean geographical distributions of strong and extreme DD episodes' frequency of occurrence (episodes yr^{-1}) are presented in Fig. 2. Results are given separately as obtained from MODIS-Terra and Aqua for the periods March 2000–February 2013 and 2003–2012, and corresponding to local late morning-to-noon (Terra) and afternoon (Aqua) conditions, respectively. It is evident a gradual reduction of frequencies from south to north, while for the strong DD episodes also appears a west to east decreasing gradient. The obtained patterns are in a very good agreement with those presented by Gkikas et al. (2013), who analyzed the regime of the intense Mediterranean DD episodes but from 2000 to 2007 and using only data from Terra. In the present analysis however, lower frequencies are found than in Gkikas et al. (2013) which are attributed to the different study periods as well as to different considerations applied to the satellite algorithm inputs (e.g. implementation of QA MODIS retrievals as discussed in Sect. 2.1.1). The decreasing south-to-north gradient of intense DD episodes' frequency, which is also in agreement with previous studies based on ground PM measurements (Querol et al., 2009b; Pey et al., 2013), model simulations (Papayannis et al., 2008) and AERONET AOD retrievals (Basart et al., 2009), can be attributed to the increasing distance from the major dust sources and to the higher precipitation amounts at the northern parts of the basin (e.g. Marrioti et al., 2002; Mehta and Yang, 2008).

The maximum frequencies (9.9 episodes yr^{-1}) of strong DD episodes are observed in the western parts of the study region, for both periods and datasets, while the corresponding values for the extreme ones (3.3 episodes yr^{-1}) are observed over the central Mediterranean Sea for MODIS-Terra (March 2000–February 2013). In general, there is similar spatial variability between Terra and Aqua, though slightly lower maximum frequencies are found for Aqua. Although dust episodes occur rarely across the northern parts of the study region (<1 and 0.5 episodes yr^{-1} for strong and extreme episodes), their occurrence proves that dust particles can be transported far away from their sources, up to the central (e.g. Klein et al., 2010) or even northern (e.g. Bègue et al., 2012) European areas under favorable meteorological conditions. A noticeable difference between the two study periods and platforms is that relatively high frequencies of extreme DD episodes are recorded in more northern latitudes in the Mediterranean Sea, i.e. up to 43° N, according to MODIS-Terra over March 2000–February 2013, while they are restricted south of 40° N parallel for MODIS-Aqua during 2003–2012. In order to investigate this difference in detail we have also applied the satellite algorithm, over the period 2003–2012, i.e. that of Aqua, using MODIS-Terra retrievals as inputs. Through this analysis (results not shown here), it is evident that there is a very good agreement between the satellite algorithm's outputs, for the periods March 2000–February 2013 and 2003–2012, revealing a constant dust episodes' regime. Therefore, the discrepancy appeared between MODIS-Terra and MODIS-Aqua spatial distributions in Fig. 2, is attributed to the diurnal variation of factors regulating the emission and transport of dust particles from the sources areas. Schepanski et al. (2009), analyzed the variation of the Saharan dust source activation throughout the day, based on MSG-SEVIRI satellite retrievals, reporting that dust mobilization is more intense in the local early morning hours after sunrise. Note, that desert dust episodes over the period March 2000–February 2013 have been identified based on observations retrieved by the Terra satellite, which flies over the study region around noon in contrast to Aqua which provides aerosol measurements at early afternoon hours.

The analysis has been repeated (results not shown here) considering only AODs associated with cloud fractions lower/equal than 0.8, in order to investigate possible modifications to our results (Figs. 2 and 3) due to the cloud contamination effect. As it concerns the strong DD episodes, the geographical distributions are similar with those of Fig. 2, but the maximum frequencies (recorded in Morocco) are higher by up to 2 episodes yr^{-1} and 0.3 episodes yr^{-1} for the MODIS-Terra (March 2000–February 2013) and MODIS-Aqua (2003–2012) data set, respectively. On the contrary, in the case of extreme DD episodes the maximum frequencies decrease to 2.5 episodes yr^{-1} for the period 2003–2012 and they shift southwards, namely over the northern coasts of Africa, while over the central parts of the Mediterranean Sea are lower than 1 episode yr^{-1}.

The maps of intensities (in terms of $AOD_{550\,nm}$) of DD episodes (Fig. 3), show that for both study periods and satellite platforms, the maximum intensities are over the Gulf of Sidra and the Libyan Sea, along the northern African coasts. These intensities reach AODs up to about 1.5 for strong and 4.1 for extreme episodes, while the minimum ones (values down to 0.25–0.46) are recorded in the northern and western Mediterranean parts. Note that dissimilar spatial patterns appear between the geographical distributions of DD episodes' frequency and intensity, indicating that these two features are determined by different factors (e.g. tracks or strength of depressions). Finally, when the cloud contamination is minimized using only AODs associated with CF lower than 0.8, then the maximum intensities are shifted southwards, across the northern Africa

ACPD
15, 27675–27748, 2015

and eastern coasts of the Mediterranean, being lower than 1 and 2 for strong and extreme DD episodes, respectively. Through the rejection of possibly overestimated AODs from the dataset, it is found that the threshold levels are decreased (mainly over the most frequently dust affected areas) since both mean and standard deviation values are lower (results not shown here). Nevertheless, even though these AODs can be overestimated, in the majority of the cases the collocated AERONET AODs are high (but lower than the satellite observations) indicating the occurrence of desert dust outbreaks as it will be shown in Sect. "Intercomparison of surface-based and satellite algorithms used for the identification of the desert dust episodes". This introductory analysis was conducted in order to specify the locations where the Mediterranean dust outbreaks occur more frequently and are more intense. Nevertheless, this paper is orientated to the description of intense Mediterranean dust outbreaks' vertical structure as well as to the detailed evaluation of the applied satellite algorithm for the identification of DD episodes, and not to emphasize on their regime, which has been thoroughly analyzed in Gkikas et al. (2013).

4.2 Evaluation of the satellite algorithm against AERONET and PM_{10} measurements

The performance of the satellite algorithm is evaluated against ground measurements from 109 AERONET (Fig. 4, orange squares) and 22 PM_{10} (green triangles) stations located in the broader Mediterranean area. This is an extended and thorough validation which exceeds largely a similar one done for the outputs of the previous version of satellite algorithm (2000–2007; Gkikas et al., 2013), but only relying on 9 AERONET stations and using AOD and volume size distribution data. Here, the comparison is repeated for the improved algorithm, being extended over a longer time period, for a much larger number of AERONET stations, and an analysis of more optical properties, namely the Ångström exponent, effective radius, single scattering albedo and asymmetry parameter is made. The evaluation is performed for both study periods and satellite platforms (March 2000–February 2013 for Terra and 2003–2012 for Aqua)

ACPD
15, 27675–27748, 2015

while the issue of possible cloud contamination is also considered. However, since the obtained results revealed a very similar performance of the algorithm for both periods and platforms, only the results for the period March 2000–February 2013 are given here.

In 46 out of 109 AERONET stations, depicted with yellow triangles in Fig. 4, have been found at least one strong or extreme dust episode, for which coincident satellite and ground measurements are available. For the specific AERONET stations and episode days, the mean values of the selected AERONET aerosol optical properties have been calculated separately for strong, extreme and all (both strong and extreme) DD episodes identified by the satellite algorithm. Subsequently, these values were compared to the corresponding ones calculated from all the available retrievals (climatological conditions, clim) collected from the 109 Mediterranean AERONET stations, during the period March 2000–February 2013, aiming at highlighting the effect of episodes on these optical properties. Additionally, in 7 AERONET stations (cyan circles in Fig. 4) the intense DD episodes have been identified from ground and the corresponding results are compared with the satellite algorithm outputs (Sect. "Intercomparison of surface-based and satellite algorithms used for the identification of the desert dust episodes"). Finally, the performance of the algorithm is also tested against surface PM_{10} measurements from 22 stations (Sect. 4.2.2).

4.2.1 AERONET

Aerosol optical depth

During the period March 2000–February 2013, 346 pixel level intense DD episodes have been identified by the satellite-based algorithm, in which coincident MODIS-Terra and AERONET retrievals are available. It should be noted that AERONET $AOD_{550\,nm}$ values have been calculated from available AERONET $AOD_{870\,nm}$ and Ångström exponent data ($\alpha_{440-870\,nm}$) by applying the Ångström equation (Ångström, 1929) to match the MODIS $AOD_{550\,nm}$. For these intense DD episodes, the comparison between the satellite and ground aerosol optical depths at 550 nm is given in Fig. 5. Two similar scatterplots with matched MODIS-AERONET data pairs are given. The first one (Fig. 5i-a) is resolved by the number of level 2 (L2) measurements of 10 km × 10 km spatial resolution from which the compared 1° × 1° level 3 (L3) AODs in the figure are derived. The second scatterplot (Fig. 5i-b) is resolved by the spatial standard deviation inside the 1° × 1° geographical cell (level 3 AODs). Both scatterplots address the issue of level 3 AOD sub-grid spatial variability, which is essential when attempting comparisons against local surface-based AOD data like the AERONET.

The overall correlation coefficient (R) between MODIS and AERONET AODs is equal to 0.505, with the satellite AODs being overestimated (bias = 0.143). From the overall scatterplots, it is evident the existence of outliers associated with small number of level 2 retrievals (< 20, blue color Fig. 5i-a) and/or high standard deviations (> 0.5, yellowish-reddish points, Fig. 5i-b) inside the L3 grid cell. This finding underlines the role of homogeneity and representativeness of L3 retrievals for the performance of MODIS AODs against AERONET. This role is better visualized in Fig. 5ii-a, where are presented the computed R values between MODIS level-3 and AERONET AODs depending on the number of L2 retrievals from which the L3 products were derived. In general, it is known that the L2 pixel counts range from 0 to 121 while in polar regions (typically around 82° latitude) the maximum count numbers can be even higher due to overlapping orbits and near nadir views intersect (Hubanks et al., 2008). It is clear from our results that the correlation coefficients are gradually and essentially improved, from 0.49 to 0.75, with increasing representativeness of MODIS AODs, i.e. increasing counts of L2 retrievals attributed. A similar improvement has been reported by Amiridis et al. (2013) who found a better agreement between MODIS/AERONET and CALIOP aerosol optical depths applying similar spatial criteria. The agreement between MODIS and AERONET also improves when the former AOD products are more spatially homogeneous, i.e. when they are characterized by smaller AOD standard deviations at the grid-level (from < 0.25 down to < 0.05, Fig. 5ii-b). However, our results also indicate that apart from increasing correlation coefficients (up to 0.7–0.8) with increasing level-

ACPD
15, 27675–27748, 2015

2 counts and decreasing standard deviations, the number of intense DD episodes is decreased dramatically (about 40–50 for more than 50 counts and standard deviation smaller than 0.05).

The successful performance of the satellite algorithm as to its capability to detect intense DD episodes is also evaluated here in another way. More specifically, the spectral variation of AODs has been derived under average aerosol load and intense dust episode (strong, extreme and all) conditions. This is because it is well established by previous studies, that the spectral variation of AOD, as indicated by the Ångström formula (Ångström, 1929), is determined by the particles' size (e.g. O'Neill et al., 2003). The results of this analysis are given in Fig. 6, where AOD boxplots have been produced at 7 wavelengths, from 340 to 1020 nm, according to all available daily AERONET measurements (orange) as well as for the corresponding retrievals during strong (cyan), extreme (red) and all DD (green) episodes, identified by the satellite algorithm (Fig. 6). It is shown that under strong DD episode conditions there is a smaller spectral decrease of median AOD levels than for "climatological" (general) conditions, whereas under extreme episode conditions the spectral decrease is further reduced.

On average conditions, the median AOD is decreased from 0.23 to 0.06, i.e. by about 4 times, from ultraviolet to near-infrared wavelengths. On the contrary, for all (both strong and extreme) DD episodes this decrease factor is only 1.45 (from 0.64 to 0.44), corresponding to substantially higher AODs at larger wavelengths. The factor of increment of mean AODs under all dust episodes conditions compared to the "climatological" ones varies from 2.6 (at 340 nm) to 6 (at 1020 nm) getting gradually higher towards longer wavelengths. In absolute terms, the increase of spectral mean AOD varies from 0.36 to 0.41, from 0.54 to 0.61 and from 0.40 to 0.43 for strong, extreme and all DD episodes, respectively, revealing small wavelength dependence. Our results are in agreement, in terms of AOD levels and spectral behaviour, with those presented by Toledano et al. (2009), who analysed the spectral dust AOD at Ouarzazate (Morocco) in the framework of the Saharan Mineral Dust Experiment (SAMUM). If analyzed separately for strong and extreme DD episodes, the median AOD spec-

ACPD
15, 27675–27748, 2015

tral decrease factors (from 340 to 1020 nm) are equal to 1.51 and 1.18, respectively. These values weighted by the contribution of strong and extreme to all episodes (81.7 and 18.3 %, respectively) yield the factor of 1.45 for all episodes.

Aerosol volume size distribution

In Fig. 7, are presented the mean aerosol volume size distributions (AVSDs) calculated from all available AERONET data (orange curve) as well as under strong (cyan curve), extreme (red curve) and all (green curve) DD episodes conditions. The results are given for March 2000–February 2013 using MODIS-Terra (346 intense DD episodes) and 2003–2012 using MODIS-Aqua (305 intense DD episodes), separately and a substantial similarity is evident. In the climatological curves, two modes are distinct centered at 0.15 µm for the fine mode and 2.24 µm for the coarse mode. There is an about equal contribution of both modes, indicating the coexistence of fine (e.g. urban aerosols) and coarse (e.g. dust aerosols) particles over the broader Mediterranean area. This result is in agreement with previous studies for the Mediterranean (e.g. Fotiadi et al., 2006; Mallet et al., 2013). However, under dust episode conditions, although the AVSD still has two modes, there is a dramatic increase of the coarse mode, which strongly dominates. More specifically, the peak of the coarse mode (radius between 1.7 and 2.24 µm) is increased by factors of about 10, 15 and 11 regardless of the period, DD episodes' category and platform used. The computed factor for all DD episodes is similar with the corresponding one (~ 10) calculated by Gkikas et al. (2013). It should be noted that the increment factors are slightly decreased when the algorithm operates only with AODs associated with cloud fractions less than 0.8 which is reasonable since possible "overestimated" retrievals are masked out from the analysis. Similar modifications in the shape of AVSD during dust outbreaks have been pointed out by several studies in the past, either for the Mediterranean region (e.g. Kubilay et al., 2003; Lyamani et al., 2005; Córdoba-Jabonero et al., 2011) or for other dust affected areas of the planet (e.g. Alam et al., 2014; Cao et al., 2014).

ACPD
15, 27675–27748, 2015

Ångström exponent and effective radius

The accuracy of the DD episodes identification method was further evaluated by also using other AERONET aerosol optical properties than AOD, namely the Ångström exponent (α) and the effective radius (r_{eff}), able to provide information about particles' size. These two parameters, especially the first one, have been widely used by many researchers in order to identify or discriminate fine and coarse particles (e.g. O'Neill et al., 2003; Fotiadi et al., 2006; Toledano et al., 2007b; Gobbi et al., 2007; Basart et al., 2009; Prats et al., 2011). For this reason, we have produced the boxplots of α (Fig. 8-i) and r_{eff} (Fig. 8-ii) values, derived by AERONET sun photometers, under climatological and intense dust episode conditions (strong, extreme and all). The appropriateness of our methodology and algorithm is confirmed by the drastic reduction of α (Fig. 8-i) and increase of r_{eff} (Fig. 8-ii) values when dust outbreaks occur. Namely, the mean α value decreases by a factor of 4.8 while the r_{eff} value increases by 2.5 times, under extreme DD episodes in the Mediterranean.

According to the boxplot statistics, when all available AERONET retrievals are considered (orange boxplot), α ranges from −0.08 to 2.51 with mean and median values equal to 1.29 and 1.38, respectively. Furthermore, the majority (> 75 %) of α values is higher than 1.04 indicating the strong presence of fine particles in the study domain. On the contrary, during intense dust episodes the statistics are totally modified. For all DD episodes (green boxplots), the mean and median values are decreased down to 0.43 and 0.27, respectively, while most of α values (> 75 %) are lower than 0.54. Similar results are found for the strong DD episodes (cyan boxplots) while for the extreme cases (red boxplots) the corresponding statistical values are equal to 0.27, 0.20 and 0.36, respectively. Similar findings were reported by Tafuro et al. (2006) who calculated a low average α value equal to 0.2 ± 0.1 during dusty days ($\text{AOD}_{440\,\text{nm}} > 0.6$) from 5 AERONET stations located in the central Mediterranean, related with transported mineral particles from the northern African deserts (Pace et al., 2006). Basart et al. (2009) analyzed AERONET retrievals provided at fine temporal resolution (15 min) from 39

ACPD
15, 27675–27748, 2015

3-D Mediterranean desert dust outbreaks

A. Gkikas et al.

stations located in the broader area of Northern Africa and Middle East and reported that "pure Saharan dust" conditions are associated with AOD>0.7 and $\alpha<0.3$, very close to our finding. The existence of coarse aerosols is also confirmed by the increase of r_{eff} values under intense DD conditions compared to the climatological levels. For all DD episodes, the 75 % of r_{eff} values is higher than 0.55 µm reaching up to 1.4 µm, while the mean and the median values are equal to about 0.73, compared to about 0.37 for the climatological conditions. These values are even higher when extreme DD episodes are concerned. Despite the overall very good performance of the satellite algorithm, there are very few cases which are misclassified, corresponding to very high and low AERONET α and r_{eff} values. The possible causes of this misclassification are discussed in Sect. "Intercomparison of surface-based and satellite algorithms used for the identification of the desert dust episodes".

Single scattering albedo and asymmetry parameter

In another step towards certifying the ability of the algorithm to identify DD episodes, the spectral variation of two key aerosol optical properties, single scattering albedo (SSA) and asymmetry parameter (g_{aer}), is also assessed in this section. In Fig. 9-i and ii are presented the spectral profiles of SSA and g_{aer}, respectively, averaged from all available AERONET observations (orange curves) as well as from the corresponding measurements during strong (cyan curves), extreme (red curves) and both (green curves) DD episodes. During intense dust outbreaks the shape and magnitude of spectral SSA and g_{aer} are modified compared to the climatological conditions. These changes are similar for the three types of episodes, and more remarkable for extreme episodes. The spectral curves of both parameters become less and more flattened during episodes for SSA and g_{aer}, respectively. For SSA, the steepening results from decreasing values in the visible and increasing values in the near-infrared (by up to 0.04, reaching 0.97 at 1020 nm). The flattening for g_{aer} arises from smaller and larger decreases in visible and near-infrared values, by up to 0.04 and 0.07, respectively. These spectral variations of SSA are typical for desert dust aerosols as it has been

ACPD
15, 27675–27748, 2015

shown by Giles et al. (2012) for five dust dominated AERONET stations, by Mallet et al. (2013) in the Mediterranean, by Ogunjobi et al. (2008) in the Western Sahara and by Cao et al. (2014) in the Eastern Asia. Declinations in the SSA values which can be encountered between regions affected by Saharan or Asian dust particles are attributed to the different mineral composition (Su and Toon, 2011). The obtained results for asymmetry parameter are in agreement with those of Kim et al. (2011), although they found even smaller spectral variation and higher g_{aer} values compared to ours, based on AERONET retrievals from four stations located in North Africa and Arabian Peninsula. Also similar spectral profile but lower g_{aer} values have been reported by Alados-Arboledas et al. (2008) during a dust episode over the southeastern parts of Spain.

Intercomparison of surface-based and satellite algorithms used for the identification of the desert dust episodes

Despite their great usefulness, satellite aerosol retrievals still suffer from uncertainties, and generally are considered as inferior to surface-based similar products, which are taken as the reference. In order to examine this degree of uncertainty and to verify the successful performance of the algorithm, we also tested using it along with AERONET retrievals. This has been made for 7 Mediterranean AERONET stations, depicted with cyan circles in Fig. 4, during the periods for which ground retrievals are available (Table 1). The selection of the AERONET stations was based on: (i) data availability (see last column of Table 1), (ii) their location (i.e. near to the Northern African and Middle East deserts) and (iii) the inclusion of sites where the aerosols' regime is complex (e.g. El Arenosillo, FORTH Crete). The intense DD episodes were identified following the methodology described in Sect. 3, but using only AOD at 870 nm, $\alpha_{440-870\,\mathrm{nm}}$ (lower/equal than 0.7) and r_{eff} (higher than 0.6) as criteria, based upon their availability from AERONET. Subsequently, the algorithm was also operated again using satellite (MODIS-Terra, OMI-Aura, EP-TOMS) input data for the days with available data in each of the 7 AERONET stations.

ACPD
15, 27675–27748, 2015

In Fig. 10, are presented the overall scatterplots between satellite and ground AODs when intense DD episodes have been identified based on the ground (left column) and the satellite (right column) algorithm. Colors in Fig. 10i-a, ii-a, iii-a represent the associated MODIS-Terra Ångström exponent, effective radius and day cloud fraction (CFD) retrievals, respectively. In Fig. 10i-b and ii-b colors represent the AERONET Ångström exponent and effective radius, respectively, while in Fig. 10iii-b represent the day cloud fraction observations derived by MODIS-Terra. Through this approach it is feasible to evaluate furthermore the performance of the satellite algorithm, specify its drawbacks and check the validity of the defined thresholds (green boxes in Fig. 1).

It is apparent that the agreement between MODIS-Terra and AERONET AODs is better when DD episodes are identified from the ground, as shown by the increased correlation coefficients (from 0.52 to 0.7), increased slopes (from 0.6 to 0.9–1.0) and decreased biases (from 0.16 to −0.03). In particular, when DD episodes are identified from space, the MODIS-Terra AOD retrievals are overestimated (bias = 0.163) with regards to AERONET, particularly at low AOD values (< 0.5). In both cases, the highest overestimations are associated with cloud fractions higher than 0.7 due to the possible contamination of the satellite AODs by clouds (Fig. 10iii-a, iii-b). Given that DD episodes' identification based on AERONET retrievals is more efficient, we have used these outputs in order to check the validity of the defined thresholds in the satellite algorithm (green boxes in Fig. 1). For each aerosol optical property, it has been calculated the percentage of intense DD episodes for which the corresponding satellite observations are below or above the defined thresholds, depending on the parameter. The results given in Table 2 are satisfactory, since the percentages range from 87 to 99 %, and confirm the validity of the defined thresholds.

The scatterplots in Fig. 10i-b and ii-b also reveal some weaknesses of the satellite-based algorithm. More specifically, it is found that for few DD episodes identified by the satellite algorithm the corresponding AERONET Ångström exponent and effective radius values are higher than 1 and smaller than 0.4, respectively. These values indicate a predominance of fine particles instead of coarse ones as it would be expected for desert dust aerosols. In order to quantify the number of misclassified pixel level intense DD episodes by the satellite algorithm, we have computed the percentage of cases for which the AERONET α values are higher than 1 (15 %) and r_{eff} values are lower than 0.4 (17.7 %). Also, we have repeated these calculations for all DD episodes (Sect. "Aerosol optical depth") and the corresponding percentages were found to be equal to 11.8 and 14.5 %, respectively. These misclassifications of the satellite algorithm occur in AERONET stations (e.g. Thessaloniki, Rome, Avignon) with a strong presence of anthropogenic aerosols (Kazadzis et al., 2007; Gobbi et al., 2007; Querol et al., 2009a; Yoon et al., 2012). Some misclassifications also occur in AERONET stations (e.g. Evora, El Arenosillo, FORTH CRETE) with mixed (natural plus anthropogenic) aerosol loads (Fotiadi et al., 2006; Toledano et al., 2007b; Hatzianastassiou et al., 2009; Pereira et al., 2011). Over these areas, there are converging air masses carrying particles of different origin, as shown by performed back-trajectories analyses (results are not shown here) using the HYSPLIT (HYbrid Single-Particle Lagrangian Integrated Trajectory) model (Draxler and Rolph, 2015).

4.2.2 PM_{10} and dust contribution

For the assessment of the satellite algorithm's performance, apart from AERONET retrievals, ground PM_{10} concentrations (µg m^{-3}) measured in 22 Mediterranean stations (green triangles in Fig. 4) have also been used.

First, for each station, the number of intense DD episodes was calculated, for which coincident satellite and ground measurements (total PM_{10}) are available (Fig. 11-i). The number of concurrent DD episodes varies from 3 to 53, being in general decreasing from southern to northern stations. For 14 out of 22 stations, where at least 10 intense DD episodes were identified by the satellite-based algorithm, we have computed the correlation coefficients between satellite AODs and surface total PM_{10} concentrations (Fig. 11-ii). The highest R values (up to 0.8) are recorded in the central and eastern parts of the Mediterranean while the lowest ones are found in the western stations. These results are in agreement with those reported by Gkikas et al. (2013) who performed a similar analysis but using data for a shorter period (2000–2007) than ours. It must be noted that the correlation coefficients are affected by outliers, because of the limited number of DD episodes in each station, highlighting the sensitiveness of the intercomparison. Such outliers can be expected when satellite-based columnar AODs and surface-based PM_{10} data are compared, since satellite AODs are representative for the whole atmospheric column in contrast to in-situ PM measurements which are more representative for the planetary boundary layer affected also by local factors. Therefore, the vertical distribution of desert dust load, as it will be presented in the next section, can determine the level of agreement between satellite AODs and surface PM concentrations. Another influencing factor can be cloud contamination of MODIS AOD.

The identification method by the satellite algorithm can be considered as correct when dust PM_{10} concentrations are higher than zero. According to this, the ratio between the number of non-zero dust PM observations and the number of DD episodes (coincident satellite-derived DD episodes and total PM_{10} measurements) for each station is defined as success score. The calculated success scores (Fig. 11-iii) vary from 68 % (Monagrega, northeastern Spain, 28 episodes) to 97 % (Boccadifalco, Sicily, 33 episodes) confirming the appropriateness of the DD episodes' identification. In the majority of stations, the contribution of dust particles to the total burden (Fig. 11-iv) is above 50 %, ranging from 44 % (Zarra, Spain) to 86.8 % (Ayia Marina, Cyprus). In order to complete our analysis we have also calculated the mean (Fig. 11-v) and the median (Fig. 11-vi) dust PM_{10} concentrations for the identified intense DD episodes in each station. The mean PM_{10} concentrations mainly vary between 20 and 50 $\mu g\, m^{-3}$, being higher in the southern stations, as expected. The minimum mean value (17 $\mu g\, m^{-3}$) was recorded in Censt (Sardinia) and the maximum one (223 $\mu g\, m^{-3}$) in Ayia Marina (Cyprus). Our values are much higher than the corresponding ones in Querol et al. (2009b), who obtained that the mean levels of mineral matter in PM_{10} during dusty days range from 8 to 23 $\mu g\, m^{-3}$ based on ground concentrations derived by 21 Mediterranean stations. These differences are reasonable since here only intense desert dust outbreaks associated with high aerosol optical depths are considered. Finally, the me-

ACPD
15, 27675–27748, 2015

dian PM_{10} concentrations are lower compared to the average ones, indicating that outliers (cases with extremely high AOD or PM_{10}) can alter the results, attributed to the fact that both parameters' (AOD and PM_{10}) distributions are not Gaussians. For this reason the highest differences are found in Finokalia (Crete) and Ayia Marina (Cyprus), where the maximum daily PM_{10} concentrations, equal to 690 and 1291 $\mu g\,m^{-3}$, respectively, were recorded during an intense dust outbreak affected the eastern Mediterranean on 24 and 25 February 2006.

4.3 Vertical structure of the Mediterranean desert dust outbreaks

The ability of the developed satellite algorithm to detect intense dust episodes has been proved adequate through the evaluation analysis against AERONET retrievals and PM_{10} concentrations. Nevertheless, its main limitation is that it uses satellite retrievals representative for the whole atmospheric column prohibiting thus the description of the vertical structure of these dust outbreaks. In order to address this issue, the CALIOP-CALIPSO retrievals are used as a complementary tool to the satellite algorithm's outputs. First, for the identified dust episodes by the satellite algorithm, the spatially and temporally collocated vertically resolved CALIOP lidar observations are selected. For these cases and for each $1^{\circ} \times 1^{\circ}$ grid cell, we have divided the lower troposphere, up to 8 km, in 16 layers of 500 m height. In this way, 14 400 boxes of $1^{\circ} \times 1^{\circ}$ surface area and 500 m height have been produced. Then, for each one of them, we have calculated the overall number of dust and polluted dust observations (hereafter named as dust) according to the aerosol subtyping scheme of the CALIOP Vertical Feature Mask (VFM). Note that dust and polluted dust were chosen because in previous studies (Mielonen et al., 2009) they were shown to be the best two defined aerosol types among the other ones classified by the CALIOP VFM. Nevertheless, in case of polluted dust, Burton et al. (2013) reported that dust particles can be mixed with marine aerosols instead of smoke or pollution as assumed by the VFM retrieval algorithm. In our study, more than 95 % of the aerosol type records were pure dust, for the collocated cases between the satellite algorithm and CALIPSO observations. In addition, in the majority of the defined boxes, the percentage of dust from the overall observations is higher than 70 %, confirming furthermore the validity of the algorithm DD episodes' identification procedure. This is an excellent proof of the successful identification of DD episodes by the satellite algorithm, since CALIOP-CALIPSO is an independent and vertically resolved platform and database. Thereby, CALIOP vertical observations were subsequently used to examine the vertical structure of dust outbreaks.

In order to analyze the intensity of desert dust outbreaks at different altitudes in the troposphere, the CALIOP data of total backscatter coefficient at 532 nm ($\beta_{532\,\mathrm{nm}}$) have been also acquired. For each box, the average $\beta_{532\,\mathrm{nm}}$ values have been calculated from all the available CALIOP measurements (day and night), for the identified intense dust episodes by the satellite algorithm. More specifically, the average $\beta_{532\,\mathrm{nm}}$ values were calculated for the dust observations based on the CALIOP VFM associated with CAD scores ranging from −100 to −20, as it has been proposed by Winker et al. (2013) for discriminating aerosol from clouds. The selection of $\beta_{532\,\mathrm{nm}}$ values instead of extinction coefficients ensures that incorrect lidar ratio assumptions in the CALIOP retrieval algorithm do not affect our results. In the literature, it has been documented that the CALIOP lidar ratio is underestimated over the northern African deserts and the surrounding areas affected by Saharan dust particles, leading to an underestimation of the columnar AOD compared to MODIS and AERONET retrievals (Redemann et al., 2012; Schuster et al., 2012). Amiridis et al. (2013) stated that an increase of the lidar ratio from 40 to 58 sr, along with a series of post-corrections in the CALIOP retrievals and the implementation of several criteria concerning the cloud coverage and the spatial representativeness, can improve substantially the agreement between MODIS-Aqua/AERONET and CALIOP observations.

It should be noted that in the present work, we have analyzed all the available CALIOP overpasses (∼ 10 000) over the study region, during the period June 2006–February 2013. For brevity reasons, however, only the obtained results based on MODIS-Terra retrievals are presented here, since similar findings are drawn for MODIS-Aqua (June 2006–December 2012). Moreover, the analysis (results are not shown here) has been made separately for the identified strong and extreme DD episodes without revealing differences in the geometrical characteristics of dust outbreaks. Nevertheless, the $\beta_{532\,\mathrm{nm}}$ values are higher for the extreme DD episodes being consistent with the discrimination of dust episodes' intensity (in terms of AOD) which is applied to the satellite algorithm. In order to facilitate the visualization of our results, for each column (1° × 1° spatial resolution) and latitudinal/longitudinal zone (1°), we have calculated the overall number of dust observations and the associated weighted averages of $\beta_{532\,\mathrm{nm}}$, depending on the projection plane (latitudinal, longitudinal and columnar), according to dust observations in each box. For both parameters, the analysis has been made on an annual and seasonal basis and the corresponding results are discussed in Sect. 4.3.1 and 4.3.2, respectively.

4.3.1 Annual

In Fig. 12, are presented the three dimensional structures of the CALIOP overall dust observations (Fig. 12-i) and the associated total backscatter coefficients at 532 nm (Fig. 12-ii), during intense dust episodes conditions, over the broader Mediterranean area, for the period June 2006–February 2013. From the latitudinal projection in Fig. 12-i, it is evident that dust particles are mainly detected between 0.5 and 6 km, and more rarely up to 8 km, between the parallels 32 and 38° N. The number of dust observations is increased at higher altitudes with increasing latitudes, up to 40° N, while the altitude range (thickness) where these records are detected is gradually reduced from 4 to 2 km. At northern latitudes, the CALIPSO dust records are drastically reduced and are mainly observed between 1 and 4 km. The ascending mode of the transported mineral particles over the Mediterranean is attributed to the prevailing low pressure systems, which mobilize and uplift dust particles from the source areas across the Sahara Desert and the Arabian Peninsula. Dust aerosols are transported over the planetary boundary layer (Hamonou et al., 1999) due to the upward movement of dry and turbid air masses (Dulac et al., 1992), while the prevailing synoptic conditions determine also the spatial and temporal characteristics of desert dust outbreaks over the Mediterranean (Gkikas et al., 2014).

In general, our results are in agreement with previous studies, based on lidar profiles, which have been made in several Mediterranean sites. More specifically, Papayannis et al. (2008) found that dust layers, over the EARLINET Mediterranean stations, extend from 0.5 to 10 km above mean sea level, their center of mass is located between 2.5 and 3.5 km and their thickness ranges from 2.1 to 3.3 km. Hamonou et al. (1999) reported that dust layers are mainly detected between 1.5 and 5 km based on lidar measurements in the northwestern and northeastern Mediterranean. According to di Sarra et al. (2001), who studied the Saharan dust intrusions in Lampedusa (central Mediterranean) for the period May–June 1999, dust particles can be detected up to 7–8 km, which is in line with our findings for the corresponding latitudinal zones (35–36° N). Balis (2012), analyzed 33 Raman/lidar profiles of Saharan dust intrusions over Thessaloniki (northern Greece), and found that the mean base and top of dust layers were equal to 2.5 ± 0.9 and 4.2 ± 1.5 km, respectively.

As to the variation of vertical extension with longitude (Fig. 12-i), it is revealed that the base height of dust layers is decreased towards the eastern parts of the study region. In the western Mediterranean, the mineral particles are mainly detected between 2 and 6 km while over the central and eastern Mediterranean the corresponding altitudes are equal to 0.5 and 6 km, respectively. It is well known, that dust is transported over the western Mediterranean mainly in summer (e.g. Moulin et al., 1998) favored by low pressure systems located over the northwestern Africa (Gkikas et al., 2014) and the enhanced thermal convection, uplifting effectively dust aerosols at high altitudes in the troposphere. Moreover, air masses carrying dust particles are “pushed” towards higher altitudes due to the existence of the Atlas Mountains Range. Therefore, the combination of strong convective processes over North Africa along with topography can explain the identification of dust aerosols at higher tropospheric levels over the western Mediterranean. It is the presence of mineral particles at high altitudes in western Mediterranean that can explain the poor-to-moderate agreement between

ACPD
15, 27675–27748, 2015

PM_{10} concentrations and MODIS AODs found in the Iberian Peninsula (Fig. 11-ii). On the contrary, air masses carrying African dust aerosols travel at lower altitudes over Africa and the central and eastern Mediterranean, because of absence of significant topographical objects on their route, as suggested by Pey et al. (2013).

Previous studies have shown that dust layers over the Mediterranean are characterized by a multilayered structure (e.g. Hamonou et al., 1999; Mona et al., 2006; Papayannis et al., 2008). This is also depicted in the longitudinal projection of Fig. 12-i, where several dust layers of different base/top altitudes and geometrical thicknesses are detected. In general, the base heights vary from 0.5 to 2 km, the top heights from 4 to 6 km and the thicknesses from 1 to 4 km. The majority of common observations between the CALIOP profiles and the identified intense DD episodes by the satellite algorithm are recorded over the maritime parts of the study region (bottom map of Fig. 12-i). The maximum number of CALIOP dust observations (~ 19 000) is recorded along the Atlantic coasts of Morocco, but high numbers (about 10 000–15 000) are also found across the northern African coasts.

Apart from the CALIOP dust observations, we have also analyzed the associated $\beta_{532\,\text{nm}}$ values at the defined altitude ranges in order to describe the variation of intensity of the desert dust episodes with height over the Mediterranean (Fig. 12-ii). The maximum backscatter coefficients (up to 0.006 $\text{km}^{-1}\,\text{sr}^{-1}$) are observed below 2 km, being increased towards the southern edges (30–34° N) of the study region, where their source areas are found. This is explained by the fact that dust particles due to their coarse size and large mass, are efficiently deposited and for this reason they are recorded at higher concentrations near to the source areas and at low altitudes. Nevertheless, the decreasing intensity with height towards the north is not so evident. Thus, high $\beta_{532\,\text{nm}}$ values (~ 0.004 $\text{km}^{-1}\,\text{sr}^{-1}$) are observed between 2 and 4 km in the latitudinal zone extending from 35 to 42° N. Though, the uppermost altitudes where relatively high $\beta_{532\,\text{nm}}$ values gradually decrease from 6 to 4 km, moving from South to North. Any differences in the latitudinal patterns of dust observations and backscatter values

ACPD
15, 27675–27748, 2015

(Fig. 12-i and ii) can be explained by the fact that $\beta_{532\,\text{nm}}$ values take into account only the dust records and not the overall observations (all aerosol types).

The decrease of backscatter values at higher altitudes has been pointed out in previous studies where lidar profiles have been analyzed over specific Mediterranean locations (e.g. Mona et al., 2006; Papayannis et al., 2008). Nevertheless, it must be considered that in the aforementioned studies the lidar measurements are valid above the retrieved planetary boundary layer (Matthias et al., 2004) which varies depending on the location and the season (McGrath-Spangler et al., 2013). Despite the good agreement, as it concerns the vertical shape of the $\beta_{532\,\text{nm}}$ curves, between our findings and the corresponding ones based on ground retrievals, in the present analysis the calculated backscatter coefficients are in general higher, which is reasonable since are considered only cases of intense desert dust outbreaks.

The longitudinal pattern of $\beta_{532\,\text{nm}}$ profiles (Fig. 12-ii) is less distinct compared to the corresponding one resulted from the latitudinal projection. Relatively high $\beta_{532\,\text{nm}}$ values ($\sim 0.004\,\text{km}^{-1}\,\text{sr}^{-1}$) are found between 1 and 5 km over the western Mediterranean, while over the central and eastern parts of the study region the desert dust outbreaks' intensity ($\sim 0.006\,\text{km}^{-1}\,\text{sr}^{-1}$) is higher below 1.5 km. Among the sub-regions, the backscatter coefficients are higher in the central and eastern Mediterranean, which is also depicted in the bottom map of Fig. 12-ii. It is reminded that higher intensities of dust episodes over the central and eastern Mediterranean have also been noticed based on MODIS retrievals (Fig. 3). From the obtained longitudinal projection, it is evident a patchy structure of the total backscatter coefficient profiles, especially in the central and eastern parts, indicating the existence of several dust layers of varying intensities at different altitudes into the atmosphere.

4.3.2 Seasonal

The vertical structure of Mediterranean desert dust outbreaks has also been analyzed separately for winter (DJF), spring (MAM), summer (JJA) and autumn (SON). The seasonal three dimensional representations of the CALIOP overall dust observations and

ACPD
15, 27675–27748, 2015

the associated total backscatter coefficients are depicted in the left and right column of Fig. 13, respectively. It must be noted, that for $\beta_{532\,\mathrm{nm}}$ the colorbars' ranges are common, depending on the projection plane. More specifically, the maximum limits have been set to 0.012, 0.014 and 0.021 $\mathrm{km}^{-1}\,\mathrm{sr}^{-1}$ for the latitudinal, longitudinal and bottom map projections, respectively. It should be mentioned that $\beta_{532\,\mathrm{nm}}$ values can reach up to 0.045 $\mathrm{km}^{-1}\,\mathrm{sr}^{-1}$, but are associated with a very small number of dust observations.

The majority (85 %) of dust observations is recorded in spring and summer, attributed to the enhanced production rates of mineral particles and the prevailing atmospheric circulation over the source areas and the Mediterranean. According to the latitudinal projections, it is evident a seasonal variability of the intense Mediterranean desert dust outbreaks' geometrical characteristics. Dust particles are detected at higher altitudes (6–7 km) during warm seasons of the year while in winter are mainly detected below 3 km and in autumn are recorded between 2 and 5 km. Nevertheless, it should be mentioned that during these seasons only a small number of pixels (see bottom maps in Fig. 13 i-a, iv-a) is available considering also that clouds prohibit the satellite observations. Note that in spring, dust can be found at low tropospheric levels while in summer it is mainly observed above 1 km highlighting thus the role of topography and the enhanced thermal convection. During the first half of the year, the maximum dust observations are confined between the parallels 31 and 37° N while during the second one, are shifted northwards in the latitudinal zone extending from 34 to 40° N. Similar latitudinal projections were also presented by Luo et al. (2015), who developed a new algorithm to improve CALIOP's ability to detect optically thin dust layers. From the longitudinal projections as well as from the bottom maps, it is evident that the maximum dust records are found in different Mediterranean sub-regions, depending on the season. The geometrical characteristics, in longitudinal terms, of intense DD episodes affecting the western, central and eastern parts of the Mediterranean are similar to those presented in the annual three dimensional structure (Fig. 12-i) being more frequent in the eastern and central Mediterranean in winter, spring and autumn and in the western and central Mediterranean in summer.

ACPD
15, 27675–27748, 2015

The seasonal patterns of $\beta_{532\,\mathrm{nm}}$ latitudinal projections are different than those for the dust observations, while they also differ among the four seasons. The intensity of winter DD episodes is stronger (up to 0.012 $km^{-1}\,sr^{-1}$) below 2 km and at the southern parts of the study region. According to the longitudinal and bottom map projections, these episodes take place over the central and eastern Mediterranean Sea but the number of grid cells with coincident CALIOP observations and DD episodes is limited. In spring, the highest $\beta_{532\,\mathrm{nm}}$ values (up to 0.006 $km^{-1}\,sr^{-1}$) are recorded between the parallels 31 and 35° N and below 2 km, although, relatively high $\beta_{532\,\mathrm{nm}}$ values (up to 0.004 $km^{-1}\,sr^{-1}$) are found up to 6 km (Fig. 13ii-b). Moving northwards, over the Mediterranean, dust layers are mainly confined between 2 and 4 km, associated with high $\beta_{532\,\mathrm{nm}}$ values (up to 0.004 $km^{-1}\,sr^{-1}$) in the latitudinal zone extending from 35 to 43° N. The existence of these elevated dust layers, has been also confirmed by model simulations through specific (Papayannis et al., 2008) or averaged (Alpert et al., 2004) cross sections of dust concentrations in the central sector of the Mediterranean. This is in accordance with our longitudinal projection (Fig. 13ii-b), where $\beta_{532\,\mathrm{nm}}$ is high varying from 0.004 to 0.008 $km^{-1}\,sr^{-1}$ at these altitude ranges.

In summer, the intensity of dust episodes is smoothly decreased at higher altitudes, where dust layers of considerable $\beta_{532\,\mathrm{nm}}$ values are also found. More specifically, the highest backscatter coefficients (up to 0.008 $km^{-1}\,sr^{-1}$) are recorded near to the surface but also moderate values (up to 0.006 $km^{-1}\,sr^{-1}$) are observed between 2 and 5 km, particularly over the southern parts of the study region (Fig. 13iii-b). Most of these intense DD episodes occur in the western Mediterranean, where the highest $\beta_{532\,\mathrm{nm}}$ values (up to 0.005 $km^{-1}\,sr^{-1}$) are recorded between 2 and 5 km. Over the central and eastern Mediterranean, even higher $\beta_{532\,\mathrm{nm}}$ values are found (up to 0.014 $km^{-1}\,sr^{-1}$) but at lower altitudes (< 1 km). In autumn, the majority of the grid cells of coincident CALIOP profiles and DD episodes identified by the satellite algorithm are located between the parallels 33 and 41° N. In this latitudinal zone, CALIOP profiles are available over the interior parts of the Iberian Peninsula and over western and central parts of the Mediterranean Sea, near to the northern African coasts. According to the latitudi-

ACPD
15, 27675–27748, 2015

nal projection, $\beta_{532\,\mathrm{nm}}$ values mainly vary from 0.002 to 0.009 $\mathrm{km^{-1}\,sr^{-1}}$, revealing an increasing tendency for increasing heights. On the contrary, the total backscatter coefficients do not show a distinct spatial pattern on the longitudinal projection, due to the limited number of grid cells participating in the calculations. Throughout the year, based on the CALIOP $\beta_{532\,\mathrm{nm}}$ retrievals, the DD episodes are more intense (up to 0.018 $\mathrm{km^{-1}\,sr^{-1}}$) in spring, when massive dust loads are transported from the Sahara desert towards the central and eastern parts of the Mediterranean Sea (bottom map in Fig. 13ii-b).

5 Summary and conclusions

This study aims at describing the vertical structure of intense desert dust outbreaks affecting the broader Mediterranean basin. To achieve this target, an updated version of an objective and dynamic algorithm, which has been introduced by Gkikas et al. (2009, 2013), has been applied for the identification of strong and extreme desert dust episodes, over the period March 2000–February 2013. For its operation, a group of optical properties, retrieved by satellite sensors (MODIS-Terra/Aqua, EP-TOMS and OMI-Aura) on a daily basis, is used, providing information about aerosols' load, size and nature. Briefly, the satellite algorithm consists of three parts; at the first one are computed the mean AOD value (Mean) and the associated standard deviation (SD) for the whole study period in each grid cell of $1^\circ \times 1^\circ$ spatial resolution, at the second one the identified aerosol episodes are classified based on their intensity to strong and extreme ones. Finally, at the third part the identified aerosol episodes are categorized as desert dust episodes, separately over land and sea. Through this approach the selected dataset consists only of intense desert dust episodes since their intensity (expressed in terms of $\mathrm{AOD}_{550\,\mathrm{nm}}$) is higher/equal than Mean + 2 · SD.

Based on the satellite algorithm's outputs, an overall view about the regime of Mediterranean desert dust outbreaks is presented for the periods March 2000–February 2013 (MODIS-Terra) and 2003–2012 (MODIS-Aqua). The main findings con-

ACPD
15, 27675–27748, 2015

cerning the intense DD episodes' frequency (in terms of episodes yr^{-1}) and intensity (in terms of AOD at 550 nm) are the following:

- Strong DD episodes occur more frequently (up to 9.9 episodes yr^{-1}) in the western Mediterranean while the extreme ones occur more frequently (up to 3.3 episodes yr^{-1}) over the central parts of the Mediterranean Sea, when the satellite algorithm operates with MODIS-Terra retrievals.
- Frequencies of occurrence of strong and extreme DD episodes are gradually reduced from south to north, while for the strong ones a west–east gradient is apparent.
- The intensity of strong and extreme DD episodes, in AOD terms, can reach up to 1.5 and 3–4, respectively, over the central and eastern parts of the Mediterranean Sea, near off the northern African coasts.
- Slightly lower frequencies and higher intensities are found for the period 2003–2012, when the satellite algorithm operates with MODIS-Aqua retrievals.
- The frequencies of occurrence and the intensities of DD episodes are slightly higher and lower, respectively, compared to the corresponding ones of the previous version of the satellite algorithm (Gkikas et al., 2013), applied for the period March 2000–February 2007, when MODIS-Terra non weighted QA retrievals were used as inputs.

Through a detailed evaluation of the satellite algorithm against surface measurements derived from 109 AERONET and 22 PM_{10} stations, it is found that:

AERONET

- The correlation coefficient between MODIS and AERONET AODs is increased from 0.505 to 0.75 when level 3 grid cells with higher sub-grid spatial representativeness and homogeneity are considered.

ACPD
15, 27675–27748, 2015

- Under intense dust episodes conditions, the spectral AERONET AOD median levels vary from 0.64 (340 nm) to 0.44 (1020 nm).
- According to the AERONET volume size distributions, it is evident the predominance of the coarse mode with a peak ($\sim 0.25\,\mu m^3\,\mu m^{-2}$) for particles radii between 1.7 and 2.24 µm, in case of intense DD episodes.
- The appropriateness of DD episodes' identification method applied to the satellite algorithm is confirmed since the majority (> 75 %) of AERONET$\alpha_{440-870\,nm}$ and r_{eff} values are lower than 0.54 and higher than 0.55 µm, respectively.
- The spectral variation of AERONET SSA and g_{aer} is found to be typical for desert dust aerosols. SSA values vary from 0.90 to 0.965 and increase (less absorption) with increasing wavelengths while g_{aer} varies from 0.704 (870 nm) to 0.742 (440 nm) revealing a reduced spectral variation.
- About 15 % of the pixel level intense DD episodes are misclassified by the satellite algorithm and these drawbacks are encountered in AERONET stations where the aerosol load is dominated either by fine particles or by complex aerosol types.

PM_{10} and dust contribution

- The agreement between surface and satellite measurements is better over the central and eastern Mediterranean stations.
- On a station level, the percentage of the intense DD episodes, for which a dust contribution to PM_{10} surface concentration has been recorded, varies from 68 % (Monagrega, northeastern Spain) to 97 % (Boccadifalco, Sicily).
- In the majority of stations, dust particles contribute more than 50 % of the total amount reaching up to 86.8 % (Ayia Marina, Cyprus).
- The mean PM_{10} concentration levels mainly vary from 20 to 50 $\mu g\,m^{-3}$ reaching up to 223 $\mu g\,m^{-3}$ in Ayia Marina (Cyprus).

ACPD
15, 27675–27748, 2015

In order to describe the vertical structure of the intense Mediterranean dust outbreaks, the CALIOP vertical profiles of aerosol subtyping and total backscatter coefficient at 532 nm, are used as a complementary tool to the identified intense DD episodes by the satellite algorithm. Through this synergistic approach it is found that:

- Dust particles are mainly detected between 0.5 and 6 km, following an ascending mode, up to 40° N, leaving from the source areas and transported towards the Mediterranean.
- Over the western Mediterranean, the dust layers are mainly observed between 2 and 6 km while their base height is decreased down to 0.5 km for increasing longitudes.
- During the warm period of the year, dust particles are uplifted at higher altitudes (up to 8 km).
- In summer, the transported dust loads over the western Mediterranean are recorded above 1 km and in spring at lower altitudes over the central and eastern parts of the study region. This behavior underlies the role of topography (e.g. Atlas Mountains) and the enhanced thermal convection.
- The intensity of dust outbreaks, in terms of $\beta_{532\,\mathrm{nm}}$, is maximized (up to $0.006\,\mathrm{km}^{-1}\,\mathrm{sr}^{-1}$) below 2 km and at the southern parts (30–34° N) of the study region.
- In spring, considerably high $\beta_{532\,\mathrm{nm}}$ values ($\sim 0.004\,\mathrm{km}^{-1}\,\mathrm{sr}^{-1}$) are observed between 2 and 4 km in the latitudinal zone extending from 35 to 42° N.
- Moderate-to-high $\beta_{532\,\mathrm{nm}}$ values are observed up to 6 km, near to the source areas, while the top of dust layers is gradually decreased down to 4 km towards northern latitudes.

– From the longitudinal projection of $\beta_{532\,\text{nm}}$, it is evident that DD episodes are more intense ($\sim 0.004\,\text{km}^{-1}\,\text{sr}^{-1}$) between 1 and 5 km in the western Mediterranean, while over the central and eastern sectors, the maximum intensities ($\sim 0.006\,\text{km}^{-1}\,\text{sr}^{-1}$) are recorded below 1.5 km.

– On a seasonal basis, DD episodes are found to be more intense (up to $0.018\,\text{km}^{-1}\,\text{sr}^{-1}$) in spring, when dust is transported towards the central and eastern parts of the Mediterranean region.

This study attempts to highlight the importance of the synergistic use of satellite observations and the usage of surface-based measurements, targeting to the representation of the 3-D structure of dust outbreaks and the description of their spatial and temporal features. For this reason, the further development of the satellite algorithm is an ongoing process by our group, aiming at extending the study domain from regional to global scale, considering the latest version of MODIS retrievals (Collection 006) as well as the Deep Blue Algorithm retrievals, available over the major dust sources of the planet.

Acknowledgement. The MDRAF project has received funding from the European Union's Seventh Framework Programme for research, technological development and demonstration under grant agreement no 622662. The Collection 051 MODIS-Terra and MODIS-Aqua data were obtained from NASA's Level 1 and Atmosphere Archive and Distribution System (LAADS) website (ftp://ladsweb.nascom.nasa.gov/). The Earth Probe (TOMS) and OMI aerosol climatology is available from the Mirador ftp server (http://mirador.gsfc.nasa.gov/). The CALIPSO retrievals have been derived from NASA's Earth Observing System Data and Information System (http://reverb.echo.nasa.gov/). We would like to thank the principal investigators maintaining the AERONET sites used in the present work. We would like to acknowledge the EMEP Programme and the public European databases Airbase and ACTRIS, which supplied PM10 data used in this study. J. Pey benefits from a Ramón y Cajal Research Grant (RYC-2013-14159) from the Spanish Ministry of Economy and Competitiveness. S. Basart, O. Jorba, S. Gassó and J. M. Baldasano acknowledge the CICYT project CGL2013-46736 and Severo Ochoa (SEV-996 2011-00067) programme of the Spanish Government. The publication was supported by the European Union Seventh Framework Programme (FP-7-REGPOT-2012-2013-1), in the framework of the project BEYOND, under Grant Agreement No. 316210 (BEYOND – Building Capacity for a Centre of Excellence for EO-based monitoring of Natural Disasters). This work is contributing to the Chemistry-Aerosol Mediterranean Experiment (ChArMEx) coordinated effort for the long-term Mediterranean aerosol characterization using available remote sensing datasets.

References

Adams, A. M., Prospero, J. M., and Zhang, C.: CALIPSO-derived three-dimensional structure of aerosol over the Atlantic Basin and adjacent continents, J. Climate, 25, 6862–6879, doi:10.1175/JCLI-D-11-00672.1, 2012.

Alados-Arboledas, A., Alcántara, A., Olmo, F. J., Martínez-Lozano, J. A., Estellés, V., Cachorro, V., Silva, A. M., Horvath, H., Gangl, A., Díaz, A., Pujadas, M., Lorente, J., Labajo, A., Sorribas, M., and Pavese, G.: Aerosol columnar properties retrieved from Cimel radiometers during VELETA 2002, Atmos. Environ., 42, 2630–2642, doi:10.1016/j.atmosenv.2007.10.006, 2008.

Alam, K., Trautmann, T., Blaschke, T., and Subhan, F.: Changes in aerosol optical properties due to dust storms in the Middle East and Southwest Asia, Remote Sens. Environ. 143, 216–227, 2014.

Alpert, P., Kishcha, P., Shtivelman, A., Krichak, S. O., and Joseph, J. H.: Vertical distribution of Saharan dust based on 2.5-year model predictions, Atmos. Res., 70, 109–130, 2004.

Amiridis, V., Kafatos, M., Perez, C., Kazadzis, S., Gerasopoulos, E., Mamouri, R. E., Papayannis, A., Kokkalis, P., Giannakaki, E., Basart, S., Daglis, I., and Zerefos, C.: The potential of the synergistic use of passive and active remote sensing measurements for the validation of a regional dust model, Ann. Geophys., 27, 3155–3164, doi:10.5194/angeo-27-3155-2009, 2009.

Amiridis, V., Wandinger, U., Marinou, E., Giannakaki, E., Tsekeri, A., Basart, S., Kazadzis, S., Gkikas, A., Taylor, M., Baldasano, J., and Ansmann, A.: Optimizing CALIPSO Saharan dust retrievals, Atmos. Chem. Phys., 13, 12089–12106, doi:10.5194/acp-13-12089-2013, 2013.

Ångström, A. K.: On the atmospheric transmission of sun radiation and on the dust in the air, Geogr. Ann. A, 12, 130–159, 1929.

Balis, D.: Geometrical characteristics of desert dust layers over Thessaloniki estimated with backscatter/Raman lidar and the BSC/DREAM model, IEEE Geosci. Remote S., 3, 353–362, doi:10.1080/01431161.2011.597793, 2012.

Balis, D., Amiridis, V., Kazadzis, S., Papayannis, A., Tsaknakis, G., Tzortzakis, S., Kalivitis, N., Vrekoussis, M., Kanakidou, M., Mihalopoulos, N., Chourdakis, G., Nickovic, S., Pérez, C., Baldasano, J., and Drakakis, M.: Optical characteristics of desert dust over the East Mediterranean during summer: a case study, Ann. Geophys., 24, 807–821, doi:10.5194/angeo-24-807-2006, 2006.

Barkan, J., Alpert, P., Kutiel, H., and Kishcha, P.: Synoptics of dust transportation days from Africa toward Italy and central Europe, J. Geophys. Res., 110, D07208, doi:10.1029/2004JD005222, 2005.

Barnaba, F. and Gobbi, G. P.: Aerosol seasonal variability over the Mediterranean region and relative impact of maritime, continental and Saharan dust particles over the basin from MODIS data in the year 2001, Atmos. Chem. Phys., 4, 2367–2391, doi:10.5194/acp-4-2367-2004, 2004.

Basart, S., Pérez, C., Cuevas, E., Baldasano, J. M., and Gobbi, G. P.: Aerosol characterization in Northern Africa, Northeastern Atlantic, Mediterranean Basin and Middle East from direct-sun AERONET observations, Atmos. Chem. Phys., 9, 8265–8282, doi:10.5194/acp-9-8265-2009, 2009.

Basart, S., Pay, M. T., Jorba, O., Pérez, C., Jiménez-Guerrero, P., Schulz, M., and Baldasano, J. M.: Aerosols in the CALIOPE air quality modelling system: evaluation and analysis of PM levels, optical depths and chemical composition over Europe, Atmos. Chem. Phys., 12, 3363–3392, doi:10.5194/acp-12-3363-2012, 2012.

Ben-Ami, Y., Koren, I., and Altaratz, O.: Patterns of North African dust transport over the Atlantic: winter vs. summer, based on CALIPSO first year data, Atmos. Chem. Phys., 9, 7867–7875, doi:10.5194/acp-9-7867-2009, 2009.

Ben-Ami, Y., Koren, I., Rudich, Y., Artaxo, P., Martin, S. T., and Andreae, M. O.: Transport of North African dust from the Bodélé depression to the Amazon Basin: a case study, Atmos. Chem. Phys., 10, 7533–7544, doi:10.5194/acp-10-7533-2010, 2010.

Bègue, N., Tulet, P., Chaboureau, J. P., Roberts, G., Gomes, L., and Mallet, M.: Long-range transport of Saharan dust over north-western Europe during EUCAARI 2008 campaign: evolution of dust optical properties by scavenging, J. Geophys. Res., 117, D17201, doi:10.1029/2012JD017611, 2012.

Berthier, S., Chazette, P., Couvert, P., Pelon, J., Dulac, F., Thieuleux, F., Moulin, C., and Pain, T.: Desert dust aerosol columnar properties over ocean and continental Africa from Lidar in-Space Technology Experiment (LITE) and Meteosat synergy, J. Geophys. Res., 111, D21202, doi:10.1029/2005JD006999, 2006.

Bollasina, M. A., Ming, Y., and Ramaswamy, V.: Anthropogenic aerosols and the weakening of the South Asian summer monsoon, Science, 334, 502–505, 2011.

Bösenberg, J., Matthias, V., Amodeo, A., Amoiridis, V., Ansmann, A., Baldasano, J. M., Balin, I., Balis, D., Böckmann, C., Boselli, A., Carlsson, G., Chaikovsky, A., Chourdakis, G., Comerón, A., De Tomasi, F., Eixmann, R., Freudenthaler, V., Giehl, H., Grigorov, I., Hågård, A., Iarlori, M., Kirsche, A., Kolarov, G., Komguem, L., Kreipl, S., Kumpf, W., Larchevêque, G., Linné, H., Matthey, R., Mattis, I., Mekler, A., Mironova, I., Mitev, V., Mona, L., Müller, D., Music, S., Nickovic, S., Pandolfi, M., Papayannis, A., Pappalardo, G., Pelon, J., Pérez, C., Perrone, R. M., Persson, R., Resendes, D. P., Rizi, V., Rocadenbosch, F., Rodrigues, J. A., Sauvage, L., Schneidenbach, L., Schumacher, R., Shcherbakov, V., Simeonov, V., Sobolewski, P., Spinelli, N., Stachlewska, I., Stoyanov, D., Trickl, T., Tsaknakis, G., Vaughan, G., Wandinger, U., Wang, X., Wiegner, M., Zavrtanik, M., and Zerefos, C.: A European aerosol research lidar network to establish an aerosol climatology, MPI-Rep. 317, Max-Planck Inst. für Meteorol., Hamburg, Germany, available at: http://www.mpimet.mpg.de/fileadmin/publikationen/Reports/max_scirep_348.pdf (last access: 6 October 2015), 2003.

Burton, S. P., Ferrare, R. A., Vaughan, M. A., Omar, A. H., Rogers, R. R., Hostetler, C. A., and Hair, J. W.: Aerosol classification from airborne HSRL and comparisons with the CALIPSO vertical feature mask, Atmos. Meas. Tech., 6, 1397–1412, doi:10.5194/amt-6-1397-2013, 2013.

Cachorro, V. E., Vergaz, R., de Frutos, A. M., Vilaplana, J. M., Henriques, D., Laulainen, N., and Toledano, C.: Study of desert dust events over the southwestern Iberian Peninsula in year 2000: two case studies, Ann. Geophys., 24, 1493–1510, doi:10.5194/angeo-24-1493-2006, 2006.

Cao, C. X., Zheng, S., and Singh, R. P.: Characteristics of aerosol optical properties and meteorological parameters during three major dust events (2005–2010) over Beijing, China, Atmos. Res., 150, 129–142, doi:10.1016/j.atmosres.2014.07.022, 2014.

Córdoba-Jabonero, C., Sorribas, M., Guerrero-Rascado, J. L., Adame, J. A., Hernández, Y., Lyamani, H., Cachorro, V., Gil, M., Alados-Arboledas, L., Cuevas, E., and de la Morena, B.: Synergetic monitoring of Saharan dust plumes and potential impact on surface: a case study

of dust transport from Canary Islands to Iberian Peninsula, Atmos. Chem. Phys., 11, 3067–3091, doi:10.5194/acp-11-3067-2011, 2011.
Di Sarra, A., Di Iorio, T., Cacciani, M., Fiocco, G., and Fuà, D.: Saharan dust profiles measured by lidar at Lampedusa, J. Geophys. Res., 106, 10335–10348, 2001.
Díaz, J., Tobías A., and Linares, C.: Saharan dust and association between particulate matter and case-specific mortality: a case crossover analysis in Madrid (Spain), J. Environ. Health, 11, doi:10.1186/1476-069X-11-11, 2012.
Draxler, R. R. and Rolph, G. D.: HYSPLIT (HYbrid Single-Particle Lagrangian Integrated Trajectory) Model access via NOAA ARL READY Website, available at: http://ready.arl.noaa.gov/HYSPLIT.php (last access: 6 October 2015), NOAA Air Resources Laboratory, Silver Spring, M D., 2015.
Dubovik, O. and King, M. D.: A flexible inversion algorithm for retrieval of aerosol optical properties from Sun and sky radiance measurements, J. Geophys. Res., 105, 20673–20696, 2000.
Dubovik, O., Smirnov, A., Holben, B. N., King, M. D., Kaufman, Y. J., and Slutsker, I.: Accuracy assessments of aerosol optical properties retrieved from AERONET sun and sky radiance measurements, J. Geophys. Res., 105, 9791–9806, 2000.
Dulac, F., Moulin, C., Lambert, C. E., Guillard, F., Poitou, J., Guelle, W., Quetel, C. R., Schneider, X., Ezat, U., and Buat-Ménard, P.: Dry deposition of mineral aerosol particles in the atmosphere: significance of the large size fraction, in: Precipitation Scavenging and Atmosphere–Surface Exchange, edited by: Schwartz, S. E. and Slinn, W. G. N., Hemisphere, Richland, Washington, 841–854, 1992.
Eck, T. F., Holben, B. N., Reid, J. S., Dubovik, O., Smirnov, A., O'Neill, N. T., Slutsker, I., and Kinne, S.: Wavelength dependence of optical depth of biomass burning, urban and desert dust aerosols, J. Geophys. Res., 104, 31333–31350, 1999.
Eguchi, K., Uno, I., Yumimoto, K., Takemura, T., Shimizu, A., Sugimoto, N., and Liu, Z.: Trans-pacific dust transport: integrated analysis of NASA/CALIPSO and a global aerosol transport model, Atmos. Chem. Phys., 9, 3137–3145, doi:10.5194/acp-9-3137-2009, 2009.
Escudero, M., Querol, X., Pey, J., Alastuey, A., Pérez, N., Ferreira, F., Alonso, S., Rodríguez, S., and Cuevas, E.: A methodology for the quantification of the net African dust load in air quality monitoring networks, Atmos. Environ., 41, 5516–5524, 2007.
Fotiadi, A., Hatzianastassiou, N., Drakakis, E., Matsoukas, C., Pavlakis, K. G., Hatzidimitriou, D., Gerasopoulos, E., Mihalopoulos, N., and Vardavas, I.: Aerosol physical and optical

properties in the Eastern Mediterranean Basin, Crete, from Aerosol Robotic Network data, Atmos. Chem. Phys., 6, 5399–5413, doi:10.5194/acp-6-5399-2006, 2006.

Giles, D. M., Holben, B. N., Eck, T. F., Sinyuk, A., Smirnov, A., Slutsker, I., Dickerson, R. R., Thompson, A. M., and Schafer, J. S.: An analysis of AERONET aerosol absorption properties and classifications representative of aerosol source regions, J. Geophys. Res., 117, D17203, doi:10.1029/2012JD018127, 2012.

Ginoux, P., Prospero, J. M., Gill, T. E., Hsu, N. C., and Zhao, M.: Global-scale attribution of anthropogenic and natural dust sources and their emission rates based on MODIS Deep Blue aerosol products, Rev. Geophys., 50, RG3005, doi:10.1029/2012rg000388, 2012.

Gkikas, A., Hatzianastassiou, N., and Mihalopoulos, N.: Aerosol events in the broader Mediterranean basin based on 7-year (2000–2007) MODIS C005 data, Ann. Geophys., 27, 3509–3522, doi:10.5194/angeo-27-3509-2009, 2009.

Gkikas, A., Hatzianastassiou, N., Mihalopoulos, N., Katsoulis, V., Kazadzis, S., Pey, J., Querol, X., and Torres, O.: The regime of intense desert dust episodes in the Mediterranean based on contemporary satellite observations and ground measurements, Atmos. Chem. Phys., 13, 12135–12154, doi:10.5194/acp-13-12135-2013, 2013.

Gkikas, A., Houssos, E. E., Lolis, C. J., Bartzokas, A., Mihalopoulos, N., and Hatzianastassiou, N.: Atmospheric circulation evolution related to desert-dust episodes over the Mediterranean, Q. J. Roy. Meteor. Soc., 141, 1634–1645, doi:10.1002/qj.2466, 2014.

Gobbi, G. P., Barnaba, F., Giorgi, R., and Santacasa, A.: Altitude-resolved properties of a Saharan dust event over the Mediterranean, Atmos. Environ., 34, 5119–5127, 2000.

Gobbi, G. P., Kaufman, Y. J., Koren, I., and Eck, T. F.: Classification of aerosol properties derived from AERONET direct sun data, Atmos. Chem. Phys., 7, 453–458, doi:10.5194/acp-7-453-2007, 2007.

Gobbi, G. P., Angelini, F., Barnaba, F., Costabile, F., Baldasano, J. M., Basart, S., Sozzi, R., and Bolignano, A.: Changes in particulate matter physical properties during Saharan advections over Rome (Italy): a four-year study, 2001–2004, Atmos. Chem. Phys., 13, 7395–7404, doi:10.5194/acp-13-7395-2013, 2013.

Hamonou, E., Chazette, P., Balis, D., Dulac, F., Schneider, X., Galani, E., Ancellet, G., and Papayannis, A.: Characterization of the vertical structure of Saharan dust export to the Mediterranean basin, J. Geophys. Res., 104, 22257–22270, 1999.

ACPD
15, 27675–27748, 2015

3-D Mediterranean desert dust outbreaks

A. Gkikas et al.

Hara, Y., Yumimoto, K., Uno, I., Shimizu, A., Sugimoto, N., Liu, Z., and Winker, D. M.: Asian dust outflow in the PBL and free atmosphere retrieved by NASA CALIPSO and an assimilated dust transport model, Atmos. Chem. Phys., 9, 1227–1239, doi:10.5194/acp-9-1227-2009, 2009.

Hatzianastassiou, N., Gkikas, A., Mihalopoulos, N., Torres, O., and Katsoulis, B. D.: Natural versus anthropogenic aerosols in the eastern Mediterranean basin derived from multiyear TOMS and MODIS satellite data, J. Geophys. Res., 114, D24202, doi:10.1029/2009JD011982, 2009.

Heinold, B., Helmert, J., Hellmuth, O., Wolke, R., Ansmann, A., Marticorena, B., Laurent, B., and Tegen, I.: Regional modeling of Saharan dust events using LM-MUSCAT: model description and case studies, J. Geophys. Res., 112, D11204, doi:10.1029/2006JD007443, 2007.

Heinold, B., Tegen, I., Schepanski, K., and Hellmuth, O.: Dust Radiative feedback on Saharan boundary layer dynamics and dust mobilization, Geophys. Res. Lett., 35, L20817, doi:10.1029/2008GL035319, 2008.

Herman, J. R., Bhartia, P. K., Torres, O., Hsu, N. C., Seftor, C. J., and Celarier, E.: Global distribution of UV-absorbing aerosols from Nimbus-7/TOMS data, J. Geophys. Res., 102, 16911–16923, 1997.

Holben, B. N., Eck, T. F., Slutsker, I., Tanré, D., Buis, J. P., Setzer, A., Vermote, E., Reagan, J. A., Kaufman, Y. J., Nakajima, T., Lavenu, F., Jankowiak, I., and Smirnov, A.: AERONET – a federated instrument network and data archive for aerosol characterization, Remote Sens. Environ., 66, 1–16, 1998.

Huang, J., Minnis, P., Lin, B., Wang, T.,Yi, Y., Hu, Y., Sun-Mack, S., and Ayers, K.: Possible influences of Asian dust aerosols on cloud properties and radiative forcing observed from MODIS and CERES, Geophys. Res. Lett., 33, L06824, doi:10.1029/2005GL024724, 2006.

Huang, J., Zhang, C., and Prospero, J. M.: African dust outbreaks: a satellite perspective of temporal and spatial variability over the tropical Atlantic Ocean, J. Geophys. Res., 115, D05202, doi:10.1029/2009JD012516, 2010.

Hubanks, P. A., King, M. D., Platnick, S. A., and Pincus, R. A.: MODIS Atmosphere L3 Gridded Product Algorithm Theoretical Basis Document, MODIS Algorithm Theoretical Basis Document No. ATBD-MOD-30 for Level-3 Global Gridded Atmosphere Products (08 D3, 08 E3, 08M3), available at: http://modis.gsfc.nasa.gov/data/atbd/atbd_mod30.pdf (last access: 6 October 2015), 2008.

ACPD
15, 27675–27748, 2015

Hunt, W. H., Winker, D. M., Vaughan, M. A., Powell, K. A., Lucker, P. L., and Weimer, C.: CALIPSO Lidar Description and Performance Assessment, J. Atmos. Ocean. Tech., 26, 1214–1228, doi:10.1175/2009JTECHA1223.1, 2009.

IPCC: Summary for Policymakers, in: Climate Change 2013: The Physical Science Basis. Contribution of Working Group I to the Fifth Assessment Report of the Intergovernmental Panel on Climate Change, edited by: Stocker, T. F., Qin, D., Plattner, G.-K., Tignor, M., Allen, S. K., Boschung, J., Nauels, A., Xia, Y., Bex, V., and Midgley, P. M., Cambridge University Press, Cambridge, UK and New York, NY, USA, 2013.

Kalivitis, N., Gerasopoulos, E., Vrekoussis, M., Kouvarakis, G., Kubilay, N., Hatzianastassiou, N., Vardavas, I., and Mihalopoulos, N.: Dust transport over the eastern Mediterranean derived from TOMS, AERONET and surface measurements, J. Geophys. Res., 112, D03202, doi:10.1029/2006JD007510, 2007.

Karanasiou, A., Moreno, N., Moreno, T., Viana, M., de Leeuw, F., and Querol, X.: Health effects from Sahara dust episodes in Europe: literature review and research gaps, Environ. Int., 15, 107–114, doi:10.1016/j.envint.2012.06.012, 2012.

Karyampudi, V. M., Palm, S. P., Reagen, J. A., Fang, H., Grant, W. B., Hoff, R. M., Moulin, C., Pierce, H. F., Torres, O., Browell, E. V., and Melfi, S. H.: Validation of the Saharan dust plume conceptual model using lidar, Meteosat and ECMWF, B. Am. Meteorol. Soc., 80, 1045–1075, 1999.

Kaufman, Y. J., Tanré, D., Remer, L. A., Vermote, E. F., Chu, A., and Holben, B. N.: Operational remote sensing of tropospheric aerosol over land from EOS Moderate-resolution Imaging Spectroradiometer, J. Geophys. Res., 102, 17051–17065, 1997.

Kaufman, Y. J., Smirnov, A., Holben, B. N., and Dubovik, O.: Baseline maritime aerosol: methodology to derive the optical thickness and the scattering properties, Geophys. Res. Lett., 28, 3251–3254, 2001.

Kaufman, Y. J., Tanre, D., Holben, B. N., Mattoo, S., Remer, L. A., Eck, T. F., Vaughan, J., and Chatenet, B.: Aerosol radiative impact on spectral solar flux at the surface, derived from principal-plane sky measurements, J. Atmos. Sci., 59, 635–646, 2002.

Kazadzis, S., Bais, A., Amiridis, V., Balis, D., Meleti, C., Kouremeti, N., Zerefos, C. S., Rapsomanikis, S., Petrakakis, M., Kelesis, A., Tzoumaka, P., and Kelektsoglou, K.: Nine years of UV aerosol optical depth measurements at Thessaloniki, Greece, Atmos. Chem. Phys., 7, 2091–2101, doi:10.5194/acp-7-2091-2007, 2007.

Kim, D., Chin, M., Yu, H., Eck, T. F., Sinyuk, A., Smirnov, A., and Holben, B. N.: Dust optical properties over North Africa and Arabian Peninsula derived from the AERONET dataset, Atmos. Chem. Phys., 11, 10733–10741, doi:10.5194/acp-11-10733-2011, 2011.

Kishcha, P., Barnaba, F., Gobbi, G. P., Alpert, P., Shtivelman, A., Krichak, S. O., and Joseph, J. H.: Vertical distribution of Saharan dust over Rome (Italy): comparison between 3-year model predictions and lidar soundings, J. Geophys. Res., 110, D06208, doi:10.1029/2004JD005480, 2005.

Klein, H., Nickovic, S., Haunold, W., Bundke, U., Nillius, B., Ebert, M., Weinbruch, S., Schuetz, L., Levin, Z., Barrie, L. A., and Bingemer, H.: Saharan dust and ice nuclei over Central Europe, Atmos. Chem. Phys., 10, 10211–10221, doi:10.5194/acp-10-10211-2010, 2010.

Kubilay, N., Cokacar, T., and Oguz, T.: Optical properties of mineral dust outbreaks over the northeastern Mediterranean, J. Geophys. Res., 108, 4666, doi:10.1029/2003JD003798, 2003.

Lau, K. M., Kim, M. K., and Kim, K. M.: Asian summer monsoon anomalies induced by direct forcing: the role of the Tibetan plateau, Clim. Dynam., 26, 855–864, 2006.

Levy, R. C., Remer, L. A., Tanré, D., Kaufman, Y. J., Ichoku, C., Holben, B. N., Livingston, J. M., Russell, P. B., and Maring, H.: Evaluation of the Moderate-Resolution Imaging Spectroradiometer (MODIS) retrievals of dust aerosol over the ocean during PRIDE, J. Geophys. Res., 108, 8594, doi:10.1029/2002JD002460, 2003.

Levy, R. C., Remer, L. A., Kleidman, R. G., Mattoo, S., Ichoku, C., Kahn, R., and Eck, T. F.: Global evaluation of the Collection 5 MODIS dark-target aerosol products over land, Atmos. Chem. Phys., 10, 10399–10420, doi:10.5194/acp-10-10399-2010, 2010.

Liu, D., Wang, Z., Liu, Z., Winker, D., and Trepte, C.: Aheight resolved global view of dust aerosols from the first year CALIPSO lidar measurements, J. Geophys. Res., 113, D16214, doi:10.1029/2007JD009776, 2008.

Liu, Z., Vaughan, M., Winker, D., Kittaka, C., Getzewich, B., Kuehn, R., Omar, A., Powell, K., Trepte, C., and Hostetler, C.: The CALIPSO Lidar Cloud and Aerosol Discrimination: version 2 Algorithm and Initial Assessment of Performance, J. Atmos. Ocean. Tech., 26, 1198–1213, doi:10.1175/2009jtecha1229.1, 2009.

Luo, T., Wang, Z., Zhang, D., Liu, X., Wang, Y., and Yuan, R.: Global dust distribution from improved thin dust layer detection using A-train satellite lidar observations, Geophys. Res. Lett., 42, 620–628, doi:10.1002/2014GL062111, 2015.

Lyamani, H., Olmo, F. J., and Alados-Arboledas, L.: Saharan dust outbreak over southeastern Spain as detected by sun photometer, Atmos. Environ., 39, 7276–7284, 2005.
Mallet, M., Tulet, P., Serça, D., Solmon, F., Dubovik, O., Pelon, J., Pont, V., and Thouron, O.: Impact of dust aerosols on the radiative budget, surface heat fluxes, heating rate profiles and convective activity over West Africa during March 2006, Atmos. Chem. Phys., 9, 7143–7160, doi:10.5194/acp-9-7143-2009, 2009.
Mallet, M., Dubovik, O., Nabat, P., Dulac, F., Kahn, R., Sciare, J., Paronis, D., and Léon, J. F.: Absorption properties of Mediterranean aerosols obtained from multi-year ground-based remote sensing observations, Atmos. Chem. Phys., 13, 9195–9210, doi:10.5194/acp-13-9195-2013, 2013.
Marrioti, A., Struglia, M. V., Zeng, N., and Lau, K.-M.: The hydrological cycle in the Mediterranean region and implications for the water budget of the Mediterranean Sea, J. Climate, 15, 1674–1690, 2002.
Matthias, V., Balis, D., Bösenberg, J., Eixmann, R., Iarlori, M.,Komguem, L., Mattis, I., Papayannis, A., Pappalardo, G., Perrone, M. R., and Wang, X.: Vertical aerosol distribution overEurope: statistical analysis of Raman lidar data from 10 European Aerosol Research Lidar Network (EARLINET) stations, J. Geophys. Res.-Atmos., 109, D18201, doi:10.1029/2004JD004638, 2004.
McGrath-Spangler, E. L. and Denning, A. S.: Global seasonal variations of midday planetary boundary layer depth from CALIPSO space-borne LIDAR, J. Geophys. Res.-Atmos., 118, 1226–1233, 2013.
Mehta, A. V. and Yang, S.: Precipitation climatology over Mediterranean Basin from ten years of TRMM measurements, Adv. Geosci., 17, 87–91, doi:10.5194/adgeo-17-87-2008, 2008.
Meloni, D., di Sarra, A., Biavati, G., DeLuisi, J. J., Monteleone, F., Pace, G., Piacentino, S., and Sferlazzo, D. M.: Seasonal behavior of Saharan dust events at the Mediterranean island of Lampedusa in the period 1999–2005, Atmos. Environ., 41, 3041–3056, doi:10.1016/j.atmosenv.2006.12.001, 2007.
Meloni, D., di Sarra, A., Monteleone, F., Pace, G., Piacentino, S., and Sferlazzo, D. M.:Seasonal transport patterns of intense Saharan dust events at the Mediterranean island of Lampedusa, Atmos. Res., 88, 134–148, doi:10.1016/j.atmosres.2007.10.007, 2008.
Middleton, N. J. and Goudie, A. S.: Saharan dust: sources and trajectories, T. I. Brit. Geogr., 26, 165–181, 2001.

Mielonen, T., Arola, A., Komppula, M., Kukkonen, J., Koskinen, J., de Leeuw, G., and Lehtinen, K. E. J.: Comparison of CALIOP level 2 aerosol subtypes to aerosol types derived from AERONET inversion data, Geophys. Res. Lett., 36, L18804, doi:10.1029/2009gl039609, 2009.

Mona, L., Amodeo, A., Pandolfi, M., and Pappalardo, G.: Saharan dust intrusions in the Mediterranean area: three years of Ramanlidar measurements, J. Geophys. Res., 111, D16203, doi:10.1029/2005JD006569, 2006.

Mona, L., Papagiannopoulos, N., Basart, S., Baldasano, J., Binietoglou, I., Cornacchia, C., and Pappalardo, G.: EARLINET dust observations vs. BSC-DREAM8b modeled profiles: 12-year-long systematic comparison at Potenza, Italy, Atmos. Chem. Phys., 14, 8781–8793, doi:10.5194/acp-14-8781-2014, 2014.

Moulin, C., Lambert, C. E., Dulac, F., and Dayan, U.: Control of atmospheric export of dust from North Africa by the North Atlantic Oscillation, Nature, 387, 691–694, 1997.

Moulin, C., Lambert, C., Dayan, U., Masson, V., Ramonet, M., Bousquet, P., Legrand, M., Balkanski, Y., Guelle, W., Marticorena, B., Bergametti, G., and Dulac, F.: Satellite climatology of African dust transport in the Mediterranean atmosphere, J. Geophys. Res., 103, 13137–13144, 1998.

Nabat, P., Somot, S., Mallet, M., Chiapello, I., Morcrette, J. J., Solmon, F., Szopa, S., Dulac, F., Collins, W., Ghan, S., Horowitz, L. W., Lamarque, J. F., Lee, Y. H., Naik, V., Nagashima, T., Shindell, D., and Skeie, R.: A 4-D climatology (1979–2009) of the monthly tropospheric aerosol optical depth distribution over the Mediterranean region from a comparative evaluation and blending of remote sensing and model products, Atmos. Meas. Tech., 6, 1287–1314, doi:10.5194/amt-6-1287-2013, 2013.

Ogunjobi, K. O., He, Z., and Simmer, C.: Spectral aerosol optical properties from AERONET Sun-photometric measurements over West Africa, Atmos. Res., 88, 89–107, doi:10.1016/j.atmosres.2007.10.004, 2008.

Omar, A. H., Winker, D. M., Kittaka, C., Vaughan, M. A., Liu, Z. Y., Hu, Y. X., Trepte, C. R., Rogers, R. R., Ferrare, R. A., Lee, K. P., Kuehn, R. E., and Hostetler, C. A.: The CALIPSO automated aerosol classification and lidar ratio selection algorithm, J. Atmos. Ocean. Tech., 26, 1994–2014, doi:10.1175/2009jtecha1231.1, 2009.

O'Neill, N. T., Eck, T. F., Smirnov, A., Holben, B. N., and Thulasiraman, S.: Spectral discrimination of coarse and fine mode optical depth, J. Geophys. Res.-Atmos., 108, 4559, doi:10.1029/2002JD002975, 2003.

Pace, G., di Sarra, A., Meloni, D., Piacentino, S., and Chamard, P.: Aerosol optical properties at Lampedusa (Central Mediterranean). 1. Influence of transport and identification of different aerosol types, Atmos. Chem. Phys., 6, 697–713, doi:10.5194/acp-6-697-2006, 2006.

Papadimas, C. D., Hatzianastassiou, N., Mihalopoulos, N., Querol, X., and Vardavas, I.: Spatial and temporal variability inaerosol properties over the Mediterranean basin based on 6-year (2000–2006) MODIS data, J. Geophys. Res., 113, D11205, doi:10.1029/2007JD009189, 2008.

Papadimas, C. D., Hatzianastassiou, N., Mihalopoulos, N., Kanakidou, M., Katsoulis, B. D., and Vardavas, I.: Assessment of the MODIS Collections C005 and C004 aerosol optical depth products over the Mediterranean basin, Atmos. Chem. Phys., 9, 2987–2999, doi:10.5194/acp-9-2987-2009, 2009.

Papayannis, A., Balis, D., Amiridis, V., Chourdakis, G., Tsaknakis, G., Zerefos, C., Castanho, A. D. A., Nickovic, S., Kazadzis, S., and Grabowski, J.: Measurements of Saharan dust aerosols over the Eastern Mediterranean using elastic backscatter-Raman lidar, spectrophotometric and satellite observations in the frame of the EARLINET project, Atmos. Chem. Phys., 5, 2065–2079, doi:10.5194/acp-5-2065-2005, 2005.

Papayannis, A., Amiridis, V., Mona, L., Tsaknakis, G., Balis, D., Bösenberg, J., Chaikovski, A., De Tomasi, F., Grigorov, I., Mattis, I., Mitev, V., Muller, D., Nickovic, S., Pérez, C., Pietruczuk, A., Pisani, G., Ravetta, F., Rizi, V., Sicard, M., Trickl, T., Wiegner, M., Gerding, M., Mamouri, R. E., D'Amico, G., and Pappalardo, G.: Systematic lidar observations of Saharan dust over Europe in the frame of EARLINET (2000–2002), J. Geophys. Res., 113, D10204, doi:10.1029/2007JD009028, 2008.

Papayannis, A., Mamouri, R. E., Amiridis, V., Kazadzis, S., Pérez, C., Tsaknakis, G., Kokkalis, P., and Baldasano, J. M.: Systematic lidar observations of Saharan dust layers over Athens, Greece in the frame of EARLINET project (2004–2006), Ann. Geophys., 27, 3611–3620, doi:10.5194/angeo-27-3611-2009, 2009.

Pereira, S. N., Wagner, F., and Silva, A. M.: Seven years of measurements of aerosol scattering properties, near the surface, in the southwestern Iberia Peninsula, Atmos. Chem. Phys., 11, 17–29, doi:10.5194/acp-11-17-2011, 2011.

Pérez, C., Nickovic, S., Pejanovic, G., Baldasano, J. M., and Özsoy, E.: Interactive dust-radiation modeling: a step to improve weather forecasts, J. Geophys. Res., 111, D16206, doi:10.1029/2005JD006717, 2006.

Pérez García-Pando, C., Stanton, M. C., Diggle, P. J., Trzaska, S., Miller, R. L., Perlwitz, J. P., Baldasano, J. M., Cuevas, E., Ceccato, P., Yaka, P., and Thomson, M. C.: Soil dust aerosols and wind as predictors of seasonal meningitis incidence in Niger, Environ. Health Persp., 122, 679–686, doi:10.1289/ehp.1306640, 2014.

Pey, J., Querol, X., Alastuey, A., Forastiere, F., and Stafoggia, M.: African dust outbreaks over the Mediterranean Basin during 2001–2011: PM_{10} concentrations, phenomenology and trends, and its relation with synoptic and mesoscale meteorology, Atmos. Chem. Phys., 13, 1395–1410, doi:10.5194/acp-13-1395-2013, 2013.

Pisani, G., Boselli, A., Spinelli, N., and Wang, X.: Characterization of Saharan dust layers over Naples (Italy) during 2000–2003 EARLINET project, Atmos. Res., 102, 286–299, doi:10.1016/j.atmosres.2011.07.012, 2011.

Prats, N., Cachorro, V. E., Berjón, A., Toledano, C., and De Frutos, A. M.: Column-integrated aerosol microphysical properties from AERONET Sun photometer over southwestern Spain, Atmos. Chem. Phys., 11, 12535–12547, doi:10.5194/acp-11-12535-2011, 2011.

Prospero, J. M. and Lamb, P. J.: African droughts and dust transport to the Caribbean: climate change mplications, Science, 302, 1024–1027, doi:10.1126/science.1089915, 2003.

Prospero, M. J., Ginoux, P., Torres, O., Nicholson, S. E., and Gill, T. E.: Environmental characterization of global sources of atmospheric soil dust identified with the Nimbus 7 Total Ozone Mapping Spectrometer (TOMS) absorbing aerosol product, Rev. Geophys., 40, 1002, doi:10.1029/2000RG000095, 2002.

Querol, X., Alastuey, A., Lopez-Soler, A., Plana, F., Puicercus, J. A., Mantilla, E., Miro, J. V., and Artiñano, B.: Seasonal evolution of atmospheric suspended particles around a coal-fired power station: particulate levels and sources, Atmos. Environ., 32, 1963–1978, 1998.

Querol, X., Alastuey, A., Pey, J., Cusack, M., Pérez, N., Mihalopoulos, N., Theodosi, C., Gerasopoulos, E., Kubilay, N., and Koçak, M.: Variability in regional background aerosols within the Mediterranean, Atmos. Chem. Phys., 9, 4575–4591, doi:10.5194/acp-9-4575-2009, 2009a.

Querol, X., Pey, J., Pandolfi, M., Alastuey, A., Cusack, M., Pérez, N., Moreno, T., Viana, N., Mihalopoulos, N., Kallos, G., and Kleanthous, S.: African dust contributions to mean ambient PM_{10} mass-levels across the Mediterranean basin, Atmos. Environ., 43, 4266–4277, doi:10.1016/j.atmosenv.2009.06.013, 2009b.

Redemann, J., Vaughan, M. A., Zhang, Q., Shinozuka, Y., Russell, P. B., Livingston, J. M., Kacenelenbogen, M., and Remer, L. A.: The comparison of MODIS-Aqua (C5) and CALIOP

ACPD
15, 27675–27748, 2015

(V2 & V3) aerosol optical depth, Atmos. Chem. Phys., 12, 3025–3043, doi:10.5194/acp-12-3025-2012, 2012.
Remer, L. A., Tanré, D., Kaufman, Y. J., Ichoku, C., Mattoo, S., Levy, R., Chu, D. A., Holben, B., Dubovik, O., Smirnov, A., Martins, J. V., Li, R.-R., and Ahman, Z.: Validation of MODIS aerosol retrieval over ocean, Geophys. Res. Lett., 29, 8008, doi:10.1029/2001GL013204, 2002.
Remer, L. A., Kaufman, Y. J., Tanré, D., Mattoo, S., Chu, D. A., Martins, J. V., Li, R. R., Ichoku, C., Levy, R. C., Kleidman, R. G., Eck, T. F., Vermote, E., and Holben, B. N.: The MODIS aerosol algorithm, products and validation, J. Atmos. Sci., 62, 947–973, doi:10.1175/JAS3385.1, 2005.
Remer, L. A., Kleidman, R. G., Levy, R. C., Kaufman, Y. J., Tanré, D., Mattoo, S., Martins, J. V., Ichoku, C., Koren, I., Yu, H., and Holben, B. N.: Global aerosol climatology from the MODIS satellite sensors, J. Geophys. Res., 113, D14S07, doi:10.1029/2007JD009661, 2008.
Rodríguez, S., Querol, X., Alastuey, A., Kallos, G., Kakaliagou, O.: Saharan dust contributions to PM_{10} and TSP levels in Southern and Eastern Spain, Atmos. Environ., 35, 2433–2447, 2001.
Salvador, P., Alonso-Pérez, S., Pey, J., Artíñano, B., de Bustos, J. J., Alastuey, A., and Querol, X.: African dust outbreaks over the western Mediterranean Basin: 11-year characterization of atmospheric circulation patterns and dust source areas, Atmos. Chem. Phys., 14, 6759–6775, doi:10.5194/acp-14-6759-2014, 2014.
Schepanski, K., Tegen, I., Todd, M. C., Heinold, B., Bonisch, G., Laurent, B., and Macke, A.: Meteorological processes forcing Saharan dust emission inferred from MSG-SEVIRI observations of subdaily dust source activation and numerical models, J. Geophys. Res., 114, D10201, doi:10.1029/2008jd010325, 2009.
Schuster, G. L., Vaughan, M., MacDonnell, D., Su, W., Winker, D., Dubovik, O., Lapyonok, T., and Trepte, C.: Comparison of CALIPSO aerosol optical depth retrievals to AERONET measurements, and a climatology for the lidar ratio of dust, Atmos. Chem. Phys., 12, 7431–7452, doi:10.5194/acp-12-7431-2012, 2012.
Smirnov, A., Holben, B. N., Eck, T. F., Dubovik, O., and Slutsker, I.: Cloud screening and quality control algorithms for the AERONET database, Remote Sens. Environ., 73, 337–349, 2000.
Solmon, F., Mallet, M., Elguindi, N., Giorgi, F., Zakey, A., and Konaré, A.: Dust aerosol impact on regional precipitation over western Africa, mechanisms and sensitivity to absorption properties, Geophys. Res. Lett., 35, L24705, doi:10.1029/2008GL035900, 2008.

Stephens, G. L., Vane, D. G., Boain, R. J., Mace, G. G., Sassen, K., Wang, Z., Illingworth, A. J., O'Conner, E. J., Rossow, W. G., Durden, S. L., Miller, S. D., Austin, R. T., Benedetti, A., and Mitrescu, C.: The CloudSat mission and the A-Train, B. Am. Meteorol. Soc., 83, 1771–1790, 2002.

Su, L. and Toon, O. B.: Saharan and Asian dust: similarities and differences determined by CALIPSO, AERONET, and a coupled climate-aerosol microphysical model, Atmos. Chem. Phys., 11, 3263–3280, doi:10.5194/acp-11-3263-2011, 2011.

Tafuro, A. M., Barnaba, F., De Tomassi, F., Perrone, M. R., and Gobbi, G. P.: Saharan dust particle properties over the Central Mediterranean, Atmos. Res., 81, 67–93, doi:10.1016/j.atmosres.2005.11.008, 2006.

Tanré, D., Kaufman, Y. J., Herman, M., and Mattoo, S.: Remote sensing of aerosol properties over oceans using the MODIS/EOS spectral radiances, J. Geophys. Res., 102, 16971–16988, 1997.

Tegen, I.: Modelling the mineral dust aerosol cycle in the climate system, Quaternary Sci. Rev., 22, 1821–1834, 2003.

Toledano, C., Cachorro, V. E., de Frutos, A. M., Sorribas, M., Prats, N., and de la Morena, B. A.: Inventory of African desert dust events over the southwestern Iberian Peninsula in 2000–2005 with an AERONET Cimel Sun Photometer, J. Geophys. Res., 112, D21201, doi:10.1029/2006JD008307, 2007a.

Toledano, C., Cachorro, V. E., Sorribas, M., Berjón, A., de la Morena, B. A., de Frutos, A. M., and Gouloub, P.: Aerosol optical depth and Ångström exponent climatology at El Arenosillo AERONET site (Huelva, Spain), Q. J. Roy. Meteor. Soc., 133, 795–807, doi:10.1002/qj.54, 2007b.

Toledano, C., Wiegner, M., Garhammer, M., Seefeldner, M., Gasteiger, J., Müller, D., and Koepke, P.: Spectral aerosol optical depth characterization of desert dust during SAMUM2006, Tellus B, 61, 216–228, doi:10.1111/j.1600-0889.2008.00382.x, 2009.

Torres, O., Bhartia, P. K., Herman, J. R., Ahmad, Z., and Gleason, J.: Derivation of aerosol properties from a satellite measurements of backscattered ultraviolet radiation: theoretical basis, J. Geophys. Res., 103, 17099–17110, 1998.

Torres, O., Bhartia, P. K., Herman, J. R., Sinyuk, A., and Holben, B.: A long term record of aerosol optical thickness from TOMS observations and comparison to AERONET measurements, J. Atmos. Sci., 59, 398–413, 2002.

ACPD
15, 27675–27748, 2015

Torres, O., Bhartia, P. K., Sinyuk, A., Welton, E. J., and Holben, D.: Total Ozone Mapping Spectrometer measurements of aerosol absorption from space: comparison to SAFARI 2000 ground-based observations, J. Geophys. Res., 110, D10S18, doi:10.1029/2004JD004611, 2005.

Torres, O., Tanskanen, A., Veihelman, B., Ahn, C., Braak, R., Bhartia, P. K., Veefkind, P., and Levelt, P.: Aerosols and Surface UV Products from OMI Observations: an overview, J. Geophys. Res., 112, D24S47, doi:10.1029/2007JD008809, 2007.

Trigo, I. F., Bigg, G. R., and Davies, T. D.: Climatology of cyclogenesis in the Mediterranean, Mon. Weather Rev., 130, 549–569, 2002.

Tsamalis, C., Chédin, A., Pelon, J., and Capelle, V.: The seasonal vertical distribution of the Saharan Air Layer and its modulation by the wind, Atmos. Chem. Phys., 13, 11235–11257, doi:10.5194/acp-13-11235-2013, 2013.

Varga, G., Ùjvári, G., and Kovács, J.: Spatiotemporal patterns of Saharan dust outbreaks in the Mediterranean Basin, Aeolian Res., 15, 151–160, doi:10.1016/j.aeolia.2014.06.005, 2014.

Vaughan, M. A., Powell, K. A., Kuehn, R. E., Young, S. A., Winker, D. M., Hostetler, C. A., Hunt, W. H., Liu, Z. Y., McGill, M. J., and Getzewich, B. J.: Fully automated detection of cloud and aerosol layers in the CALIPSO lidar measurements, J. Atmos. Ocean. Tech., 26, 2034–2050, doi:10.1175/2009jtecha1228.1, 2009.

Winker, D., Vaughan, M., Omar, A., Hu, Y., Powell, K., Liu, Z., Hunt, W., and Young, S.: Overview of the CALIPSO mission and CALIOP data processing algorithm, J. Atmos. Ocean. Tech., 26, 2310–2323, doi:10.1175/2009JTECHA1281.1, 2009.

Winker, D. M., Tackett, J. L., Getzewich, B. J., Liu, Z., Vaughan, M. A., and Rogers, R. R.: The global 3-D distribution of tropospheric aerosols as characterized by CALIOP, Atmos. Chem. Phys., 13, 3345–3361, doi:10.5194/acp-13-3345-2013, 2013.

Yoon, J., von Hoyningen-Huene, W., Kokhanovsky, A. A., Vountas, M., and Burrows, J. P.: Trend analysis of aerosol optical thickness and Ångström exponent derived from the global AERONET spectral observations, Atmos. Meas. Tech., 5, 1271–1299, doi:10.5194/amt-5-1271-2012, 2012.

Zhang, J. L., Reid, J. S., and Holben, B. N.: An analysis of potential cloud artifacts in MODIS over ocean aerosol optical thickness products, Geophys. Res. Lett., 32, L15803, doi:10.1029/2005GL023254, 2005.

Zhang, L., Li, Q. B., Gu, Y., Liou, K. N., and Meland, B.: Dust vertical profile impact on global radiative forcing estimation using a coupled chemical-transport–radiative-transfer model, Atmos. Chem. Phys., 13, 7097–7114, doi:10.5194/acp-13-7097-2013, 2013.

Table 1. AERONET stations, depicted with cyan colors in Fig. 4, which have been used for the identification of desert dust (DD) episodes based on ground retrievals.

Stations	Latitude	Longitude	Study period
Blida	N 36°30′28″	E 02°52′51″	7 Nov 2003–18 Feb 2012
El Arenosillo	N 37°06′18″	W 06°43′58″	1 Mar 2000–21 Feb 2010
Evora	N 38°34′04″	W 07°54′43″	4 Jul 2003–28 Feb 2013
FORTH CRETE	N 35°19′58″	E 25°16′55″	23 Jan 2003–6 Aug 2011
IMC Oristano	N 39°54′36″	E 08°30′00″	30 May 2000–28 Feb 2003
IMS METU Erdemli	N 36°33′54″	E 34°15′18″	1 Mar 2000–28 Feb 2013
Nes Ziona	N 31°55′19″	E 34°47′20″	1 Feb 2000–28 Feb 2013

ACPD
15, 27675–27748, 2015

Table 2. Percentages of the satellite Ångström exponent, Fine fraction, Effective Radius and Aerosol Index retrievals satisfying the defined thresholds in the satellite algorithm for the identification of desert dust episodes.

Parameter	Valid	Invalid	Number of DD episodes
Ångström exponent	97.8 %	2.2 %	232
Fine fraction	98.7 %	1.3 %	232
Effective radius	94.5 %	5.5 %	117
Aerosol Index	86.9 %	13.1 %	206

ACPD
15, 27675–27748, 2015

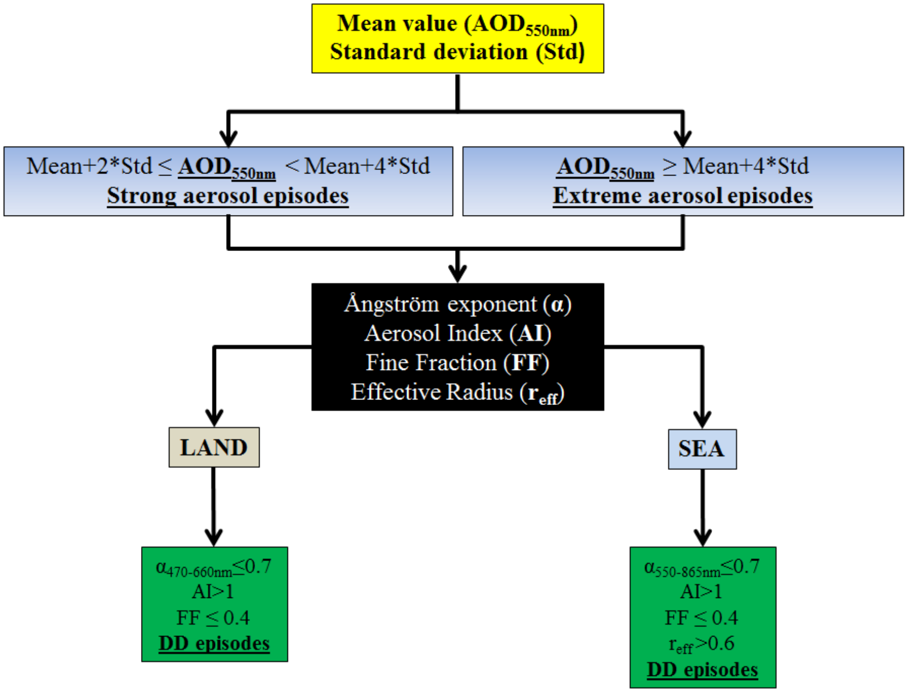

Figure 1. Methodology flowchart for the identification of the intense Mediterranean desert dust outbreaks.

ACPD
15, 27675–27748, 2015

3-D Mediterranean desert dust outbreaks

A. Gkikas et al.

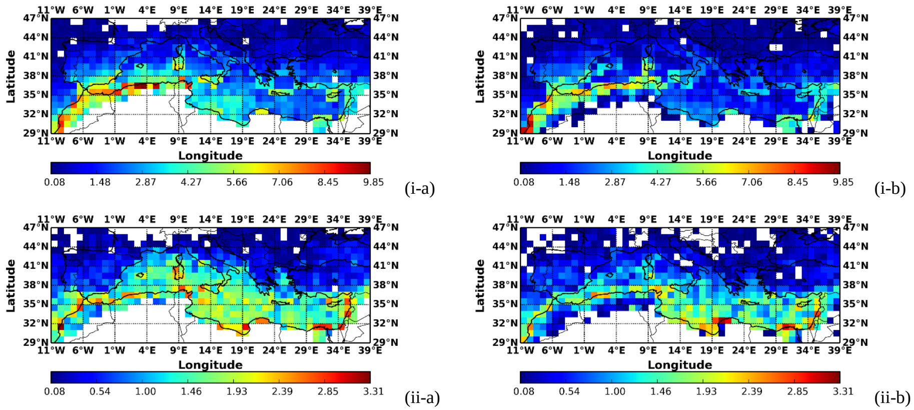

Figure 2. Geographical distributions of the occurrence frequency (episodes/year) of: **(i)** strong and **(ii)** extreme desert dust episodes, averaged for the periods: **(a)** March 2000–February 2013 (MODIS-Terra) and **(b)** 2003–2012 (MODIS-Aqua), over the broader area of the Mediterranean basin.

ACPD
15, 27675–27748, 2015

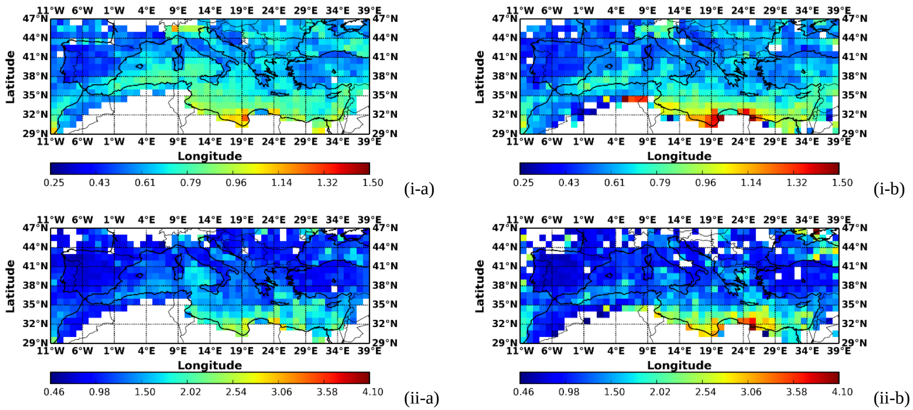

Figure 3. Geographical distributions of the intensity (in terms of $AOD_{550\,nm}$) of: **(i)** strong and **(ii)** extreme desert dust episodes, averaged for the periods: **(a)** 2000–2013 and **(b)** 2003–2012, over the broader area of the Mediterranean basin.

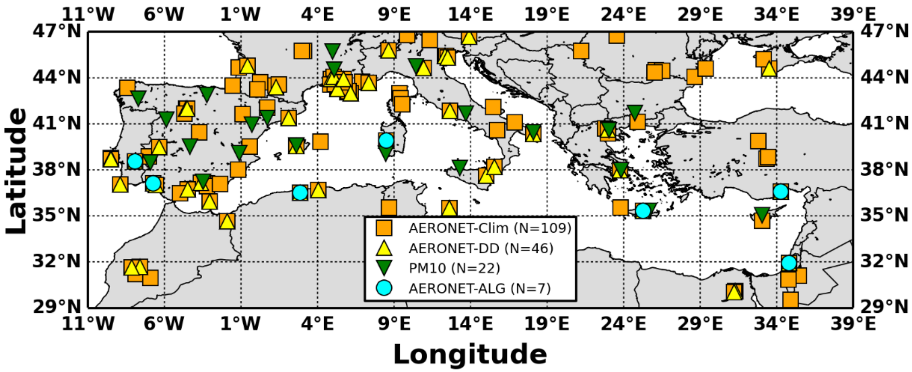

Figure 4. Locations of the AERONET and PM_{10} stations which have been used for the evaluation of the algorithm's outputs. More specifically, with orange squares are denoted the AERONET stations located into the study region, with the yellow triangles the AERONET stations with coincident satellite and ground retrievals under dust episodes conditions, with the cyan circles the AERONET stations which have been used for the evaluation of the defined algorithm thresholds and with the green triangles are depicted the PM_{10} stations.

ACPD
15, 27675–27748, 2015

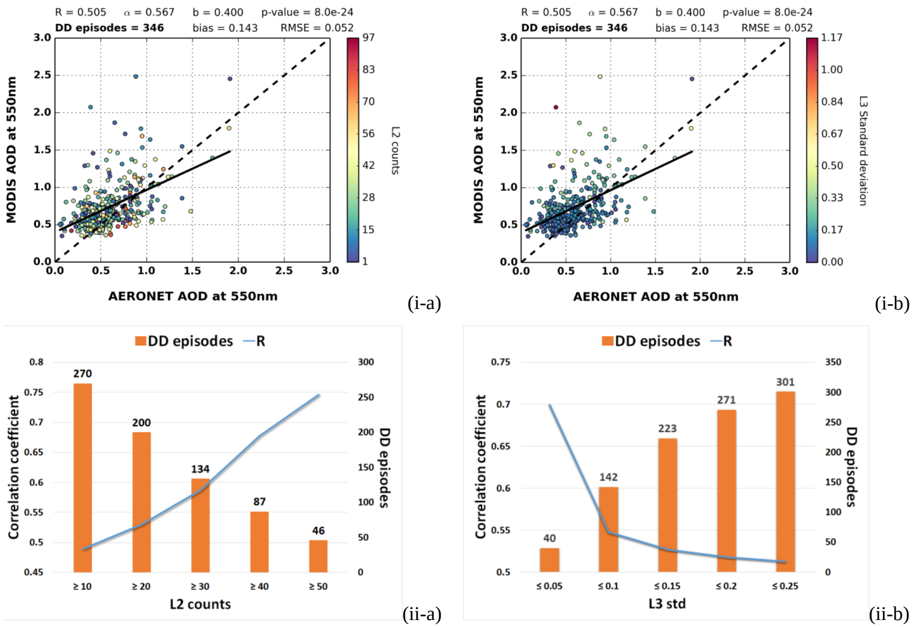

Figure 5. (i) Scatterplots between MODIS-Terra and AERONET aerosol optical depths at 550 nm under intense desert dust episodes conditions related to the: **(a)** number of level 2 counts which are used for the calculation of the level 3 retrievals and **(b)** spatial standard deviation inside the $1^{\circ} \times 1^{\circ}$ grid cells (level 3 retrievals). **(ii)** Sensitivity analysis for the calculated correlation coefficients between satellite and ground AODs, depending on the: **(a)** number of level 2 retrievals and **(b)** sub-grid standard deviation of level 3 retrievals.

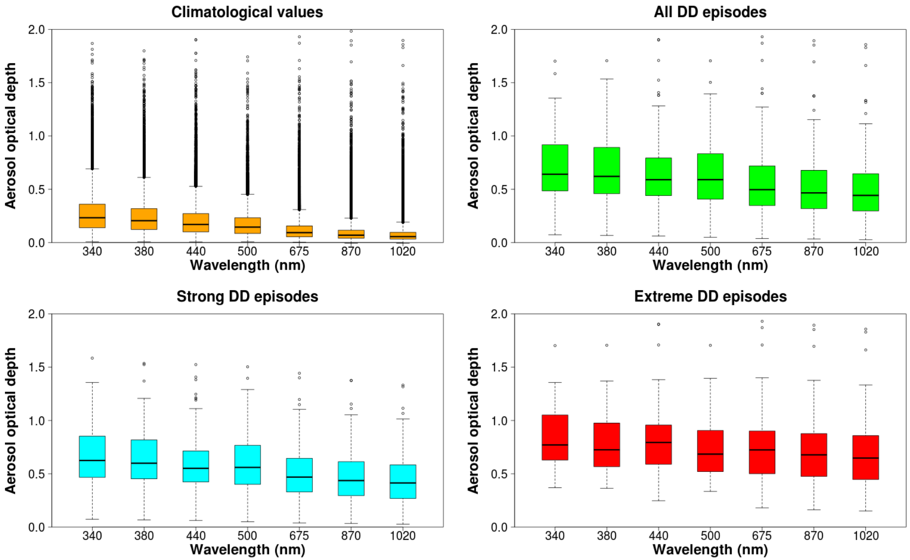

Figure 6. Spectral variation of the climatological AERONET AOD retrievals (orange, N = 54 147) as well as their corresponding values for the overall (green, N = 346), strong (cyan, N = 283) and extreme (red, N = 63) DD episodes which have been identified by the satellite algorithm.

ACPD
15, 27675–27748, 2015

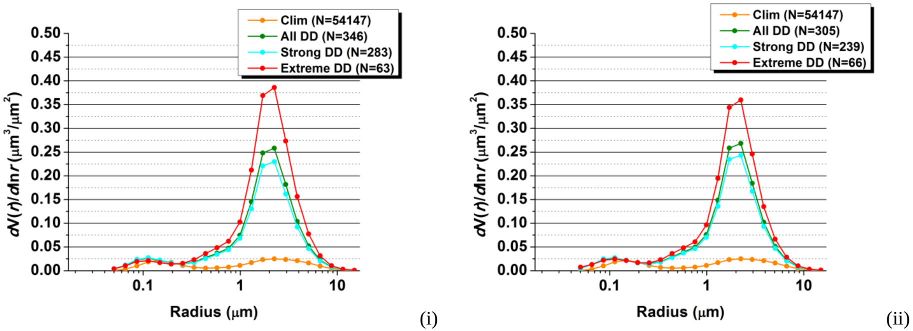

Figure 7. AERONET size distributions averaged for all available retrievals (orange curve) as well as for the total (green curve), strong (cyan curve) and extreme (red curve) desert dust episodes, occurred over the broader area of the Mediterranean basin, during the periods: **(i)** March 2000–February 2013 and **(ii)** 2003–2012.

ACPD
15, 27675–27748, 2015

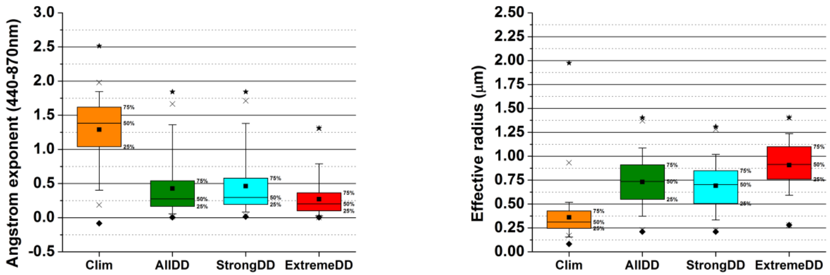

(i) (ii)

Figure 8. Boxplots of AERONET: **(i)** $\alpha_{440-870\,\mathrm{nm}}$ and **(ii)** r_{eff} retrievals calculated from all the available data (orange color) as well as from the corresponding measurements for all (green color), strong (cyan color) and extreme (red color) desert dust episodes identified over the Mediterranean, during the period March 2000–February 2013.

ACPD
15, 27675–27748, 2015

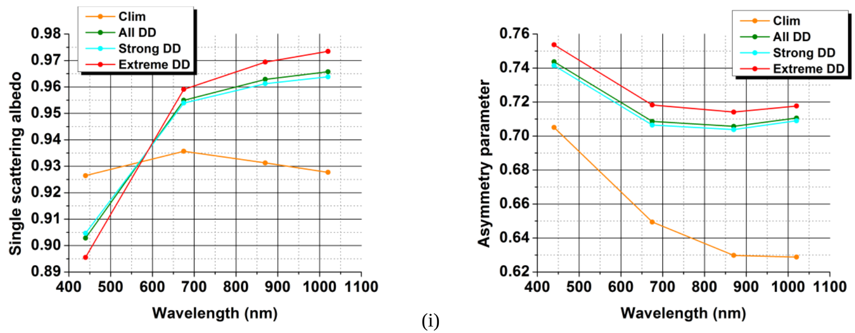

(i) (ii)

Figure 9. Spectral variation of the averaged: **(i)** single scattering albedo and **(ii)** asymmetry parameter retrievals, provided by the AERONET database, for the whole study period (orange curve) as well as for all (green curve), strong (cyan curve) and extreme (red curve) dust episodes, identified over the Mediterranean, during the period March 2000–February 2013.

ACPD
15, 27675–27748, 2015

3-D Mediterranean desert dust outbreaks

A. Gkikas et al.

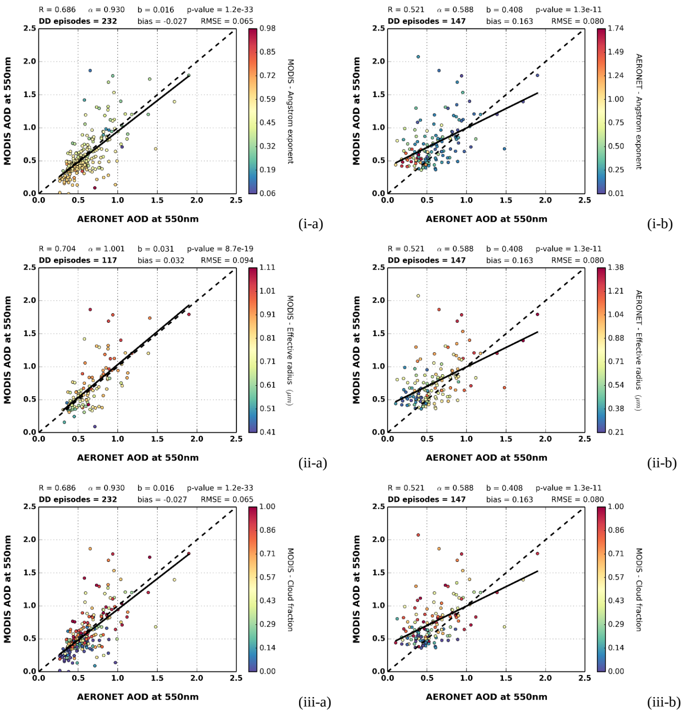

Figure 10. Scatterplots of MODIS-Terra and AERONET aerosol optical depths at 550 nm when intense dust episodes have been identified based on: **(a)** AERONET retrievals and **(b)** satellite algorithm, respectively. In the left column, colormaps indicate the corresponding values of: **(i)** Ångström exponent, **(ii)** effective radius and **(iii)** day cloud fraction derived by MODIS-Terra retrievals. In the right column, colormaps indicate the corresponding values of: **(i)** AERONET Ångström exponent, **(ii)** AERONET Effective radius and **(iii)** MODIS day cloud fraction retrievals. For each scatterplot, are provided the correlation coefficient (R), slope (α), intercept (b), p value, number of DD episodes, bias and root mean square error (RMSE).

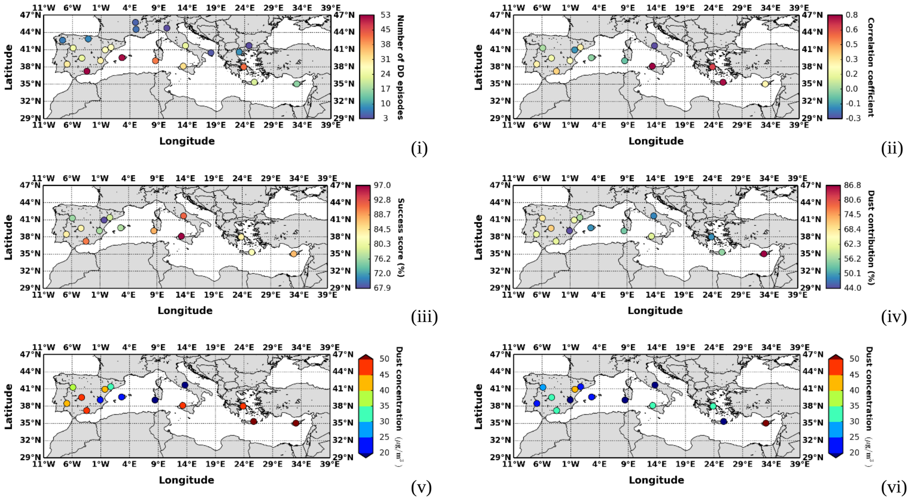

Figure 11. (i) number of concurrent intense DD episodes where total PM_{10} concentrations and MODIS-Terra AOD retrievals are available, **(ii)** computed correlation coefficient values between total PM_{10} concentrations and MODIS-Terra AOD retrievals in stations where at least 10 DD episodes have been recorded, **(iii)** percentage of intense DD episodes where dust particles have been identified by the ground stations, **(iv)** dust contribution percentages (%) to the total PM_{10} concentrations, **(v)** calculated mean and **(vi)** median dust concentrations ($\mu g\, m^{-3}$), based on ground measurements for the identified intense DD episodes by the satellite algorithm.

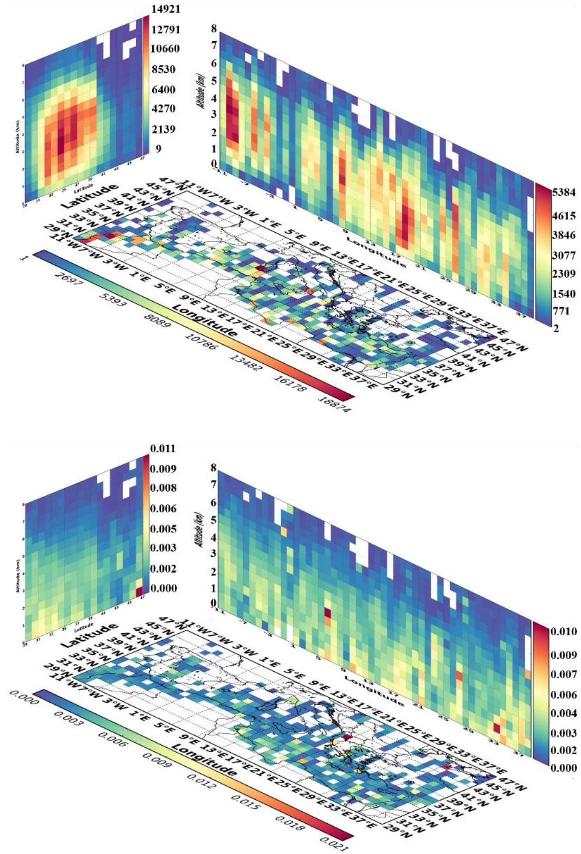

(i)

(ii)

Figure 12. Three dimensional structure of the: **(i)** overall number of dust and polluted dust observations and **(ii)** total backscatter coefficient at 532 nm, over the broader Mediterranean basin, based on CALIOP-CALIPSO vertical resolved retrievals for the period 2006–2013.

ACPD
15, 27675–27748, 2015

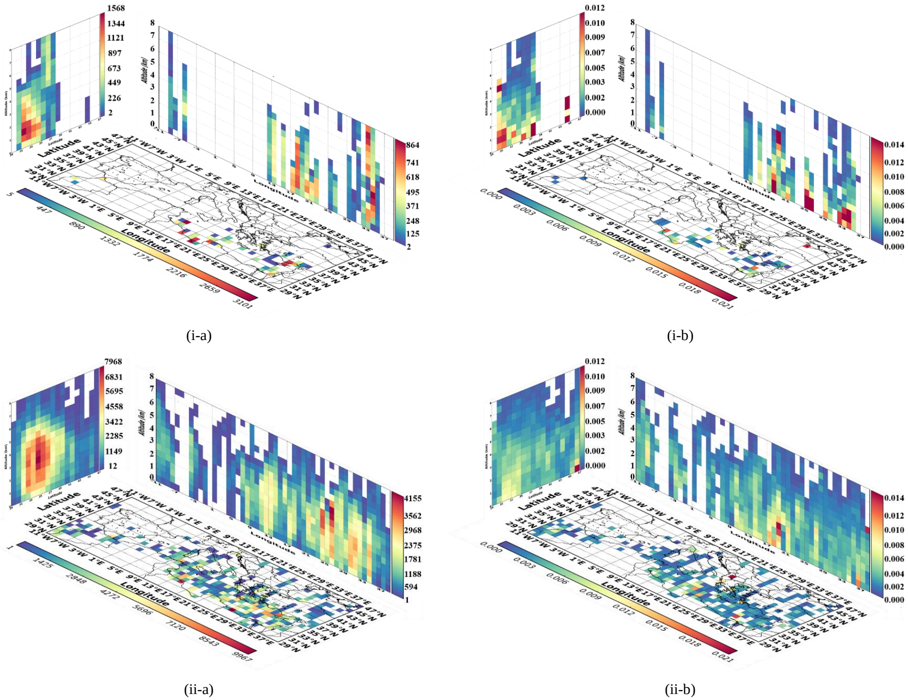

Figure 13.

ACPD
15, 27675–27748, 2015

Title Page
Abstract | Introduction
Conclusions | References
Tables | Figures
◀◀ | ▶▶
◀ | ▶
Back | Close
Full Screen / Esc
Printer-friendly Version
Interactive Discussion

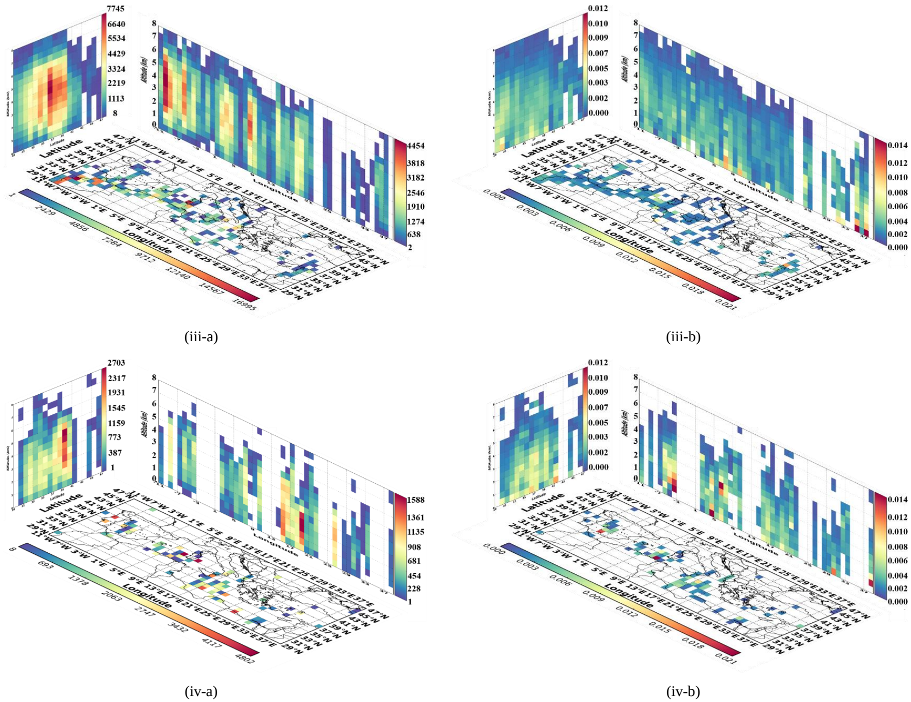

Figure 13. Three dimensional representation of the: **(a)** overall number of dust and polluted dust observations and **(b)** total backscatter coefficient at 532 nm, over the broader Mediterranean basin, for: **(i)** winter, **(ii)** spring, **(iii)** summer and **(iv)** autumn based on CALIOP-CALIPSO vertical resolved retrievals, over the period June 2006–February 2013.

ACPD
15, 27675–27748, 2015

3-D Mediterranean desert dust outbreaks

A. Gkikas et al.

Title Page
Abstract Introduction
Conclusions References
Tables Figures
◀ ▶
Back Close
Full Screen / Esc
Printer-friendly Version
Interactive Discussion